PERGAMON

International Journal of Solids and Structures 37 (2000) 4149–4179

INTERNATIONAL JOURNAL OF SOLIDS and STRUCTURES

www.elsevier.com/locate/ijsolstr

A coupled micro–macromechanical analysis of hygrothermoelastic composites

Jacob Aboudi [a,*], Todd O. Williams [b]

[a] *Faculty of Engineering, Tel-Aviv University, Ramat-Aviv, 69978, Israel*
[b] *Theoretical Division, T-3, Los Alamos National Laboratory, Los Alamos, New Mexico 87545, USA*

Received 19 February 1999; in revised form 13 April 1999

Abstract

A micro–macromechanical procedure is developed to establish the response of multiphase composites whose constituents behave, in general, as hygrothermoelastic materials. The response of the single phase is governed by the fully coupled theory of heat, moisture and deformation, and the micromechanical theory provides the hygrothermoelastic behavior of the composite. Results are presented to illustrate the effects of coupling between temperature, moisture and stress, and the interaction between the phases on the overall temporal and spatial response of a composite slab.

Keywords: Hygrothermoelasticity; Diffusion; Micromechanics; Composite materials

1. Introduction

Polymer matrix composites are susceptible to temperature and moisture changes. Thus, due to the environmental effects, the moisture content and the temperature of the composite change with position and time. Consequently, extensive investigations have been performed to study the hygrothermal effects on this type of composite, see the three volumes of collected works edited by Springer (1981, 1984, 1988), and the recent review article (that contains about 200 references) by Weitsman (1995) for example. Most of these investigations consider the diffusion process to be controlled by the classical Fick's law which ignores the coupling between the temperature, mass diffusion and mechanical deformation. Indeed observed deviations from the Fickian behavior is attributed to several factors, one of which is the omission of coupling (Sih et al., 1986).

* Corresponding author. Fax: +972-3-640-7617.
E-mail address: aboudi@eng.tau.ac.il (J. Aboudi).

0020-7683/00/$ - see front matter
PII: S0020-7683(99)00145-6

Sih et al. (1986) and Weitsman (1987) derived from the principles of continuum mechanics and irreversible thermodynamics, the governing coupled equations of hygrothermoelastic monolithic isotropic materials. In the special case when the influence of moisture is neglected, these equations provide the standard coupled thermoelastic equations. As is shown by these authors, the mechanical deformation can have significant effects on the temperature and moisture concentration fields.

In composite materials the effect of mechanical deformation upon the diffusion and temperature would be complicated by the heterogeneity and anisotropy of the system. Although such a coupled theory can be derived for anisotropic hygrothermoelastic materials, the number of parameters involved would be exceedingly large and their determination might be formidable. This can be achieved, however, by employing a micromechanical approach which provides the overall hygrothermoelastic behavior of the composite from that of the individual phases.

In the present paper, the fully coupled hygrothermoelastic equations of monolithic materials are employed in order to micromechanically establish the global behavior of multiphase composites. Thus, it is assumed, in general, that each phase is governed by the coupled theory of heat, moisture and deformation, and the overall behavior of the composite is sought. In the special case in which the diffusion equation is decoupled from the governing equations, the Fickian diffusion behavior is readily obtained.

The present derivation is based on a micro–macromechanical theory, that was previously established for the analysis of functionally graded materials (Aboudi et al., 1994). The accuracy of this theory was verified by Pindera and Dunn (1997) and Goldberg and Hopkins (1995) by comparison of the predicted results with finite element and boundary element methods, respectively. This theory is extended here and generalized to accommodate the coupled effects of temperature, moisture and mechanical deformation, and the interactions between the constituents, in order to predict the response of hygrothermoelastic multiphase composites. The micro–macromechanical theory is based on the satisfaction of the coupled hygrothermoelastic equations in the individual phases, and the interfacial continuity conditions on the tractions, displacements, heat and moisture fluxes, temperature, chemical potential, and the applied boundary conditions, all of which are satisfied in the average sense.

Results are presented for a homogeneous slab whose boundaries are subjected to a sudden application of temperature or moisture. The obtained response illustrates the effect of coupling and the type of boundary conditions on the resulting field. Results are further generated for a slab filled with a porous material and with a slab that consists of a particulate composite. In both cases the computed average hygrothermoelastic field illustrates the effect of coupling and type of boundary conditions on the structural response. It is also shown that the heat transfer and diffusion process can be significantly accelerated or decelerated by controlling the composite applied stresses.

2. Constitutive behavior of the monolithic hygrothermoelastic material

We consider in this paper composite materials in which the phases are hygrothermoelastic. Thus, the material behavior of every constituent is governed by the coupled theory of heat, moisture and mechanical deformation. The coupled constitutive equations, based on the principles of continuum mechanics and irreversible thermodynamics, were established by Sih et al. (1986) and Weitsman (1987). Here we follow the presentation of Sih et al. (1986) due to the availability of the material parameters that are involved in this formulation.

For an isotropic material with infinitesimal strains the hygrothermoelastic constitutive law is given by

$$\sigma_{ij} = \lambda \epsilon_{kk} \delta_{ij} + 2\mu_{ij} - (3\lambda + 2\mu)[\alpha(T - T_0) + \eta(C - C_0)]\delta_{ij} \tag{1}$$

where σ_{ij} and ϵ_{ij} are the stress and strain tensor components, T and C are the temperature and moisture concentration, λ and μ are the Lamé constants of the material, α and η are the linear thermal expansion and linear moisture expansion coefficients. In Eq. (1), δ_{ij} is the Kronecker delta, and T_0, C_0 are the initial state of the temperature and moisture concentration. It should be noted that in this paper summation is implied on repeated Latin indices, but no summation is implied on repeated Greek letters.

In the absence of body forces, the mechanical equilibrium equations are given by

$$\sigma_{ij,\,j} = 0 \tag{2}$$

The heat and moisture flux vectors are given, respectively, by (Sih et al., 1986)

$$\mathbf{q} = -\left(L_{21}d_t + \frac{L_{22}}{T_0}\right)\nabla T - L_{21}d_c\nabla C + L_{21}\eta\nabla\sigma_{kk} \tag{3}$$

$$\mathbf{f} = -\left(L_{11}d_t + \frac{L_{12}}{T_0}\right)\nabla T - L_{11}d_c\nabla C + L_{11}\eta\nabla\sigma_{kk} \tag{4}$$

where L_{ij}, d_c, d_t are material parameters ($L_{12} = L_{21}$).

The coupled heat conduction equation that results from the conservation of energy has the following form

$$\rho c_{\mathrm{p}}\frac{\partial T}{\partial t} - T_0 d_t\frac{\partial C}{\partial t} + T_0\alpha\frac{\partial\sigma_{kk}}{\partial t} = -q_{i,\,i} \tag{5}$$

where ρ is the material density, c_{p} is the specific heat capacity for constant moisture concentration and pressure, and t is the time.

The coupled diffusion equation which expresses the law of mass conservation is given by

$$\frac{\partial C}{\partial t} = -f_{i,\,i} \tag{6}$$

The combined relations (1)–(6) form the coupled equations that govern the behavior of the monolithic hygrothermoelastic material.

3. Model geometry

Fig. 1(a) describes a model for a multiphase composite material that consists of various regions in the form of inclusions embedded in a matrix. By adjusting the geometrical dimensions of the inclusions, continuous fibers that extend along the x_2 and x_3 can also be obtained from this model. The geometric model of this heterogeneous system is taken to have a finite thickness H, and extends to infinity in the x_2–x_3 plane. The composite is assumed to possess a periodic structure in the x_2- and x_3-directions. In the direction of the x_1-axis on the other hand, the microstructure spacing between adjacent arrays may vary. This heterogeneous composite is constructed by using the building block or generic unit cell shown in Fig. 1(b). This generic cell consists of eight subcells designated by the triplet (α, β, γ). Each index takes on the values 1 or 2 which indicate the relative position of the given subcell along the x_1-, x_2- and x_3-axes, respectively. The dimensions of the generic cell along the x_2- and x_3-axes, h_1, h_2, and l_1, l_2, are fixed for the given configuration since these are the periodic direction. On the other hand, the dimensions along the x_1-axis $d_1^{(p)}$, $d_2^{(p)}$, can vary from one generic cell to another. The dimensions of the subcells within a given cell along the x_1-direction are assigned with a running index p which

identifies the cell number. We note that p remains constant in the x_2–x_3 plane. For the other two directions, x_2 and x_3, the corresponding indices q and r are introduced. Thus, a given generic cell is designed by the triplet (p, q, r) for $p = 1, 2, \ldots, M$, where M denotes the total number of generic cells in the thickness direction x_1, and an infinite range of q and r due to the periodicity of the composite in the x_2- and x_3-directions. This implies that

$$H = \sum_{p=1}^{M} (d_1^{(p)} + d_2^{(p)})$$

For $p = 2, \ldots, M-1$ the cells are internal, whereas for $p = 1$ and $p = M$ they are boundary cells.

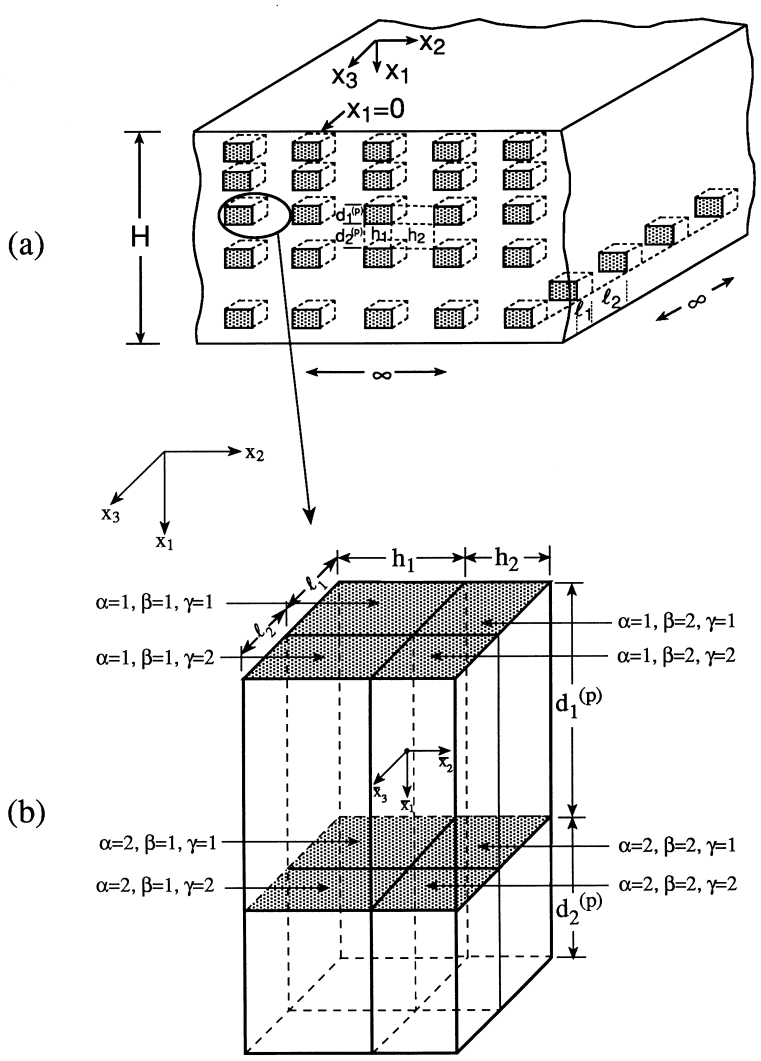

Fig. 1. (a) A model for multiphase composites that consists of a matrix and embedded inclusions. (b) The generic cell (building block) that consists of eight subcells.

It should be emphasized that the generic cell in the present framework is not taken to be a representative volume element whose effective properties can be obtained through homogenization. Thus, the response of each generic cell is explicitly coupled to the response of the entire column of cells that extends in the x_1-direction. The average behavior of the multiphase composite is determined by averaging the specific desired field quantity (e.g. the stress in 1-direction) over all general cells ($p = 1,\ldots,M$). Thus, the present model allows a coupling between the micro and macro effects which is in stark contrast with the standard uncoupled RVE-based micromechanics approach.

4. Formulation

The derived micro–macromechanical model is based on the satisfaction of the governing equations (1)–(6) in each subcell, the fulfillment of the various interfacial conditions that are described below, and the satisfaction of the appropriate boundary conditions. To this end, let us introduce a system of local coordinates ($\bar{\mathbf{x}}^{(\alpha)}$, $\bar{\mathbf{x}}^{(\beta)}$, $\bar{\mathbf{x}}^{(\gamma)}$) centered at the subcell's mid-point, see Fig. 1(b).

4.1. Traction continuity conditions

The continuity of tractions separating adjacent subcells within the generic cell (p, q, r) is fulfilled by requiring

$$\sigma_{1i}^{(1\beta\gamma)}\Big|_{\bar{x}_1^{(1)}=d_1^{(p)}/2}^{(p,\,q,\,r)} = \sigma_{1i}^{(2\beta\gamma)}\Big|_{\bar{x}_1^{(2)}=-d_2^{(p)}/2}^{(p,\,q,\,r)} \tag{7a}$$

$$\sigma_{2i}^{(\alpha1\gamma)}\Big|_{\bar{x}_2^{(1)}=h_1/2}^{(p,\,q,\,r)} = \sigma_{2i}^{(\alpha2\sigma)}\Big|_{\bar{x}_2^{(2)}=-h_2/2}^{(p,\,q,\,r)} \tag{7b}$$

$$\sigma_{3i}^{(\alpha\beta1)}\Big|_{\bar{x}_3^{(1)}=l_1/2}^{(p,\,q,\,r)} = \sigma_{3i}^{(\alpha\beta2)}\Big|_{\bar{x}_3^{(2)}=-l_2/2}^{(p,\,q,\,r)} \tag{7c}$$

In addition to the above continuity conditions within the pth generic cell, the traction continuity at the interfaces between neighboring cells are fulfilled by satisfying

$$\sigma_{1i}^{(1\beta\gamma)}\Big|_{\bar{x}_1^{(1)}=-d_1^{(p+1)}/2}^{(p+1,\,q,\,r)} = \sigma_{1i}^{(2\beta\gamma)}\Big|_{\bar{x}_1^{(2)}=d_2^{(p)}/2}^{(p,\,q,\,r)} \tag{8a}$$

$$\sigma_{2i}^{(\alpha1\gamma)}\Big|_{\bar{x}_2^{(1)}=-h_1/2}^{(p,\,q+1,\,r)} = \sigma_{2i}^{(\alpha2\gamma)}\Big|_{\bar{x}_2^{(2)}=h_2/2}^{(p,\,q,\,r)} \tag{8b}$$

$$\sigma_{3i}^{(\alpha\beta1)}\Big|_{\bar{x}_3^{(1)}=-l_1/2}^{(p,\,q,\,r+1)} = \sigma_{3i}^{(\alpha\beta2)}\Big|_{\bar{x}_3^{(2)}=l_2/2}^{(p,\,q,\,r)} \tag{8c}$$

4.2. Displacement continuity conditions

Just like the traction continuity conditions stated above, the following displacement continuity conditions must be satisfied at the interfaces within a generic cell (p, q, r) and its neighboring cells

$$\mathbf{u}^{(1\beta\gamma)}\Big|_{\bar{x}_1^{(1)}=d_1^{(p)}/2}^{(p,\,q,\,r)} = \mathbf{u}^{(2\beta\gamma)}\Big|_{\bar{x}_1^{(2)}=-d_2^{(p)}/2}^{(p,\,q,\,r)} \tag{9a}$$

$$\mathbf{u}^{(\alpha 1\gamma)}\big|^{(p,\,q,\,r)}_{\bar{x}_2^{(1)}=h_1/2} = \mathbf{u}^{(\alpha 2\gamma)}\big|^{(p,\,q,\,r)}_{\bar{x}_2^{(2)}=-h_2/2} \tag{9b}$$

$$\mathbf{u}^{(\alpha\beta 1)}\big|^{(p,\,q,\,r)}_{\bar{x}_3^{(1)}=l_1/2} = \mathbf{u}^{(\alpha\beta 2)}\big|^{(p,\,q,\,r)}_{\bar{x}_3^{(2)}=-l_2/2} \tag{9c}$$

where $\mathbf{u}^{(\alpha\beta 1)}=(u_1^{(\alpha\beta\gamma)},\, u_2^{(\alpha\beta\gamma)},\, u_3^{(\alpha\beta\gamma)})$ denotes the displacement vector in subcell $(\alpha\beta\gamma)$, and

$$\mathbf{u}^{(1\beta\gamma)}\big|^{(p+1,\,q,\,r)}_{\bar{x}_1^{(1)}=-d_1^{(p+1)}/2} = \mathbf{u}^{(2\beta\gamma)}\big|^{(p,\,q,\,r)}_{\bar{x}_1^{(2)}=d_2^{(p)}/2} \tag{10a}$$

$$\mathbf{u}^{(\alpha 1\gamma)}\big|^{(p,\,q+1,\,r)}_{\bar{x}_2^{(1)}=-h_1/2} = \mathbf{u}^{(\alpha 2\gamma)}\big|^{(p,\,q,\,r)}_{\bar{x}_2^{(2)}=h_2/2} \tag{10b}$$

$$\mathbf{u}^{(\alpha\beta 1)}\big|^{(p,\,q,\,r+1)}_{\bar{x}_3^{(1)}=-l_1/2} = \mathbf{u}^{(\alpha\beta 2)}\big|^{(p,\,q,\,r)}_{\bar{x}_3^{(2)}=l_2/2} \tag{10c}$$

4.3. Heat flux continuity conditions

The continuity of the heat flux at the interfaces of a generic cell, and between neighboring cells are satisfied by

$$q_1^{(1\beta\gamma)}\big|^{(p,\,q,\,r)}_{\bar{x}_1^{(1)}=d_1^{(p)}/2} = q_1^{(2\beta\gamma)}\big|^{(p,\,q,\,r)}_{\bar{x}_1^{(2)}=-d_2^{(p)}/2} \tag{11a}$$

$$q_2^{(\alpha 1\gamma)}\big|^{(p,\,q,\,r)}_{\bar{x}_2^{(1)}=h_1/2} = q_2^{(\alpha 2\gamma)}\big|^{(p,\,q,\,r)}_{\bar{x}_2^{(2)}=-h_2/2} \tag{11b}$$

$$q_3^{(\alpha\beta 1)}\big|^{(p,\,q,\,r)}_{\bar{x}_3^{(1)}=l_1/2} = q_3^{(\alpha\beta 2)}\big|^{(p,\,q,\,r)}_{\bar{x}_3^{(2)}=-l_2/2} \tag{11c}$$

and

$$q_1^{(1\beta\gamma)}\big|^{(p+1,\,q,\,r)}_{\bar{x}_1^{(1)}=-d_1^{(p+1)}/2} = q_1^{(2\beta\gamma)}\big|^{(p,\,q,\,r)}_{\bar{x}_1^{(2)}=d_2^{(p)}/2} \tag{12a}$$

$$q_2^{(\alpha 1\gamma)}\big|^{(p,\,q+1,\,r)}_{\bar{x}_2^{(1)}=-h_1/2} = q_2^{(\alpha 2\gamma)}\big|^{(p,\,q,\,r)}_{\bar{x}_2^{(2)}=h_2/2} \tag{12b}$$

$$q_3^{(\alpha\beta 1)}\big|^{(p,\,q,\,r+1)}_{\bar{x}_3^{(1)}=-l_1/2} = q_3^{(\alpha\beta 2)}\big|^{(p,\,q,\,r)}_{\bar{x}_3^{(2)}=l_2/2} \tag{12c}$$

4.4. Temperature continuity conditions

The continuity of the temperature at the interfaces of a generic cell, and between neighboring cells are satisfied by

$$T^{(1\beta\gamma)}\big|^{(p,\,q,\,r)}_{\bar{x}_1^{(1)}=d_1^{(p)}/2} = T^{(2\beta\gamma)}\big|^{(p,\,q,\,r)}_{\bar{x}_1^{(2)}=-d_2^{(p)}/2} \tag{13a}$$

$$T^{(\alpha 1\gamma)}\,|^{(p,\,q,\,r)}_{\bar{x}_2^{(1)}=h_1/2} = T^{(\alpha 2\gamma)}\,|^{(p,\,q,\,r)}_{\bar{x}_2^{(2)}=-h_2/2} \tag{13b}$$

$$T^{(\alpha\beta 1)}\,|^{(p,\,q,\,r)}_{\bar{x}_3^{(1)}=l_1/2} = T^{(\alpha\beta 2)}\,|^{(p,\,q,\,r)}_{\bar{x}_3^{(2)}=-l_2/2} \tag{13c}$$

and

$$T^{(1\beta\gamma)}\,|^{(p+1,\,q,\,r)}_{\bar{x}_1^{(1)}=-d_1^{(p+1)}/2} = T^{(2\beta\gamma)}\,|^{(p,\,q,\,r)}_{\bar{x}_1^{(2)}=d_2^{(p)}/2} \tag{14a}$$

$$T^{(\alpha 1\gamma)}\,|^{(p,\,q+1,\,r)}_{\bar{x}_2^{(1)}=-h_1/2} = T^{(\alpha 2\gamma)}\,|^{(p,\,q,\,r)}_{\bar{x}_2^{(2)}=h_2/2} \tag{14b}$$

$$T^{(\alpha\beta 1)}\,|^{(p,\,q,\,r+1)}_{\bar{x}_3^{(1)}=-l_1/2} = T^{(\alpha\beta 2)}\,|^{(p,\,q,\,r)}_{\bar{x}_3^{(2)}=l_2/2} \tag{14c}$$

4.5. Moisture flux continuity conditions

The continuity of the moisture flux at the interfaces of a generic cell, and between neighboring cells are satisfied by

$$f_1^{(1\beta\gamma)}\,|^{(p,\,q,\,r)}_{\bar{x}_1^{(1)}=d_1^{(p)}/2} = f_1^{(2\beta\gamma)}\,|^{(p,\,q,\,r)}_{\bar{x}_1^{(2)}=-d_2^{(p)}/2} \tag{15a}$$

$$f_2^{(\alpha 1\gamma)}\,|^{(p,\,q,\,r)}_{\bar{x}_2^{(1)}=h_1/2} = f_2^{(\alpha 2\gamma)}\,|^{(p,\,q,\,r)}_{\bar{x}_2^{(2)}=-h_2/2} \tag{15b}$$

$$f_3^{(\alpha\beta 1)}\,|^{(p,\,q,\,r)}_{\bar{x}_3^{(1)}=l_1/2} = f_3^{(\alpha\beta 2)}\,|^{(p,\,q,\,r)}_{\bar{x}_3^{(2)}=-l_2/2} \tag{15c}$$

and

$$f_1^{(1\beta\gamma)}\,|^{(p+1,\,q,\,r)}_{\bar{x}_1^{(1)}=-d_1^{(p+1)}/2} = f_1^{(2\beta\gamma)}\,|^{(p,\,q,\,r)}_{\bar{x}_1^{(2)}=d_2^{(p)}/2} \tag{16a}$$

$$f_2^{(\alpha 1\gamma)}\,|^{(p,\,q+1,\,r)}_{\bar{x}_2^{(1)}=-h_1/2} = f_2^{(\alpha 2\gamma)}\,|^{(p,\,q,\,r)}_{\bar{x}_2^{(2)}=h_2/2} \tag{16b}$$

$$f_3^{(\alpha\beta 1)}\,|^{(p,\,q,\,r+1)}_{\bar{x}_3^{(1)}=-l_1/2} = f_3^{(\alpha\beta 2)}\,|^{(p,\,q,\,r)}_{\bar{x}_3^{(2)}=l_2/2} \tag{16c}$$

4.6. Chemical potential continuity conditions

The chemical potential must be continuous across the various interfaces. This condition provides the necessary interfacial continuity condition that the moisture concentration must fulfill. It implies that at a state of thermodynamic equilibrium the moisture concentrations across an interface are related in the form

$$C\,|_1 = K(T,\,\sigma_{ij},\,C\,|_2) \tag{17}$$

where K is a function of the temperature, stresses and moisture concentration. For small amounts of moisture contents it is possible to rewrite Eq. (17) as a simple linear relationship between the concentrations across the interface as follows

$$C\,|_1 = K(T, \sigma_{ij})C\,|_2$$

For an isotropic material the chemical potential varies linearly with σ_{kk} (Sih et al., 1986; Weitsman, 1987). Hence, this function can be linearly expressed in terms of σ_{kk}, namely

$$K \simeq K_1(T) + K_2(T)\sigma_{kk} \tag{18}$$

where $K_1(T)$ and $K_2(T)$ are appropriate parameters which are temperature dependent. Consequently, the interfacial boundary conditions for the moisture concentrations can be written in the form

$$C^{(1\beta\gamma)}\,|^{(p,\,q,\,r)}_{\bar{x}_1^{(1)}=d_2^{(p)}/2} = KC^{(2\beta\gamma)}\,|^{(p,\,q,\,r)}_{\bar{x}_1^{(2)}=-d_2^{(p)}/2} \tag{19a}$$

$$C^{(\alpha 1\gamma)}\,|^{(p,\,q,\,r)}_{\bar{x}_2^{(1)}=h_1/2} = KC^{(\alpha 2\gamma)}\,|^{(p,\,q,\,r)}_{\bar{x}_2^{(2)}=-h_2/2} \tag{19b}$$

$$C^{(\alpha\beta 1)}\,|^{(p,\,q,\,r)}_{\bar{x}_3^{(1)}=l_1/2} = KC^{(\alpha\beta 2)}\,|^{(p,\,q,\,r)}_{\bar{x}_3^{(2)}=-l_2/2} \tag{19c}$$

and

$$C^{(1\beta\gamma)}\,|^{(p+1,\,q,\,r)}_{\bar{x}_1^{(1)}=-d_2^{(p+1)}/2} = KC^{(2\beta\gamma)}\,|^{(p,\,q,\,r)}_{\bar{x}_1^{(2)}=d_2^{(p)}/2} \tag{20a}$$

$$C^{(\alpha 1\gamma)}\,|^{(p,\,q+1,\,r)}_{\bar{x}_2^{(1)}=-h_1/2} = KC^{(\alpha 2\gamma)}\,|^{(p,\,q,\,r)}_{\bar{x}_2^{(2)}=h_2/2} \tag{20b}$$

$$C^{(\alpha\beta 1)}\,|^{(p,\,q,\,r+1)}_{\bar{x}_3^{(1)}=-l_1/2} = KC^{(\alpha\beta 2)}\,|^{(p,\,q,\,r)}_{\bar{x}_3^{(2)}=l_2/2} \tag{20c}$$

where for the simplicity of notation, the same function K has been assumed to control all types of interfaces.

4.7. Boundary conditions

The final set of conditions that the solution must satisfy are the boundary conditions at the top ($x_1 = 0$) and bottom ($x_1 = H$) surfaces, as well as the far field normal stress conditions in the periodic 2- and 3-directions (Aboudi et al., 1995).

Suppose, for example, that the temperature is specified on both surfaces. It follows that

$$T^{(1\beta\gamma)}\,|^{(1,\,q,\,r)} = T^{(\beta\gamma)}_{\text{top}}, \quad \bar{x}_1^{(1)} = -d_1^{(1)}/2$$

$$T^{(2\beta\gamma)}\,|^{(M,\,q,\,r)} = T^{(\beta\gamma)}_{\text{bottom}}, \quad \bar{x}_1^{(2)} = d_2^{(M)}/2$$

Other types of thermal boundary conditions can be easily formulated. Similarly, mechanical and moisture boundary conditions can be imposed in the same manner.

As to the far field boundary conditions, these will be dealt with in the following section.

5. Analysis

The micro–macromechanical analysis is based on the approximation of the displacement, temperature and moisture concentration fields in each subcell of a generic cell in terms of the corresponding field of the center of the subcell and a quadratic expansion in the local coordinates ($\bar{\mathbf{x}}^{(\alpha)}$, $\bar{\mathbf{x}}^{(\beta)}$, $\bar{\mathbf{x}}^{(\gamma)}$). The coefficients or microvariables associated with these expansions are determined by the satisfaction of the governing equations and the interfacial and boundary conditions in an average volumetric sense.

5.1. Mechanical analysis

The displacement components $u_i^{(\alpha\beta\gamma)}$ in the subcell $(\alpha\beta\gamma)$ of the generic cell (p, q, r) is approximated by a second-order expansion in the local coordinates $\bar{x}_1^{(\alpha)}$, $\bar{x}_2^{(\beta)}$ and $\bar{x}_3^{(\gamma)}$

$$u_1^{(\alpha\beta\gamma)} = w_1^{(\alpha\beta\gamma)} + \bar{x}_1^{(\alpha)}\phi_1^{(\alpha\beta\gamma)} + \tfrac{1}{2}(3\bar{x}_1^{(\alpha)2} - \tfrac{1}{4}d_{\alpha}^{(p)2})U_1^{(\alpha\beta\gamma)} + \tfrac{1}{2}(3\bar{x}_2^{(\beta)2} - \tfrac{1}{4}h_{\beta}^2)V_1^{(\alpha\beta\gamma)} + \tfrac{1}{2}(3\bar{x}_3^{(\gamma)2} - \tfrac{1}{4}l_{\gamma}^2)W_1^{(\alpha\beta\gamma)} \tag{21}$$

$$u_2^{(\alpha\beta\gamma)} = w_2^{(\alpha\beta\gamma)}(\mathbf{x}) + \bar{x}_2^{(\beta)}\chi_2^{(\alpha\beta\gamma)} \tag{22}$$

$$u_3^{(\alpha\beta\gamma)} = w_3^{(\alpha\beta\gamma)}(\mathbf{x}) + \bar{x}_3^{(\gamma)}\psi_3^{(\alpha\beta\gamma)} \tag{23}$$

where $w_i^{(\alpha\beta\gamma)}$, which are the displacements at the center of the subcell, and the microvariables $U_1^{(\alpha\beta\gamma)}$, $V_1^{(\alpha\beta\gamma)}$, $W_1^{(\alpha\beta\gamma)}$, $\phi_1^{(\alpha\beta\gamma)}$, $\chi_2^{(\alpha\beta\gamma)}$, $\psi_3^{(\alpha\beta\gamma)}$ must be determined from the coupled governing equations (2)–(6) in the subcells, in conjunction with the interfacial and boundary conditions that were given in Section 4.

It should be noted that Eq. (21) does not contain linear terms in the local coordinates $\bar{x}_2^{(\beta)}$ and $\bar{x}_3^{(\gamma)}$. This follows directly from the assumed periodicity in the 2- and 3-directions and the symmetry with respect to the fiber–matrix and matrix–matrix cross sections, see Fig. 1(a). The displacement field in the 2- and 3-directions, on the other hand, is approximated using a linear expansion in local coordinates to reflect the symmetry and the periodic character of the composite's microstructure in the x_2–x_3 plane. In addition functions of the global coordinates $\mathbf{x}=(x_1, x_2, x_3)$ are included to allow for non-zero average normal strains $\bar{\epsilon}_{22}$ and $\bar{\epsilon}_{33}$, Aboudi et al. (1995). It has been shown in this paper that the following relations hold

$$\bar{\epsilon}_{22} = \frac{\partial w_2^{(\alpha\beta\gamma)}}{\partial x_2}$$

$$\bar{\epsilon}_{33} = \frac{\partial w_3^{(\alpha\beta\gamma)}}{\partial x_3}$$

where $\bar{\epsilon}_{22}$ and $\bar{\epsilon}_{33}$ are the far field average normal strains, and they are related to the local strain as follows

$$\bar{\epsilon}_{22} = \frac{1}{V}\sum_{p=1}^{M}\sum_{\alpha,\ \beta,\ \gamma=1}^{2} v_{(\alpha\beta\gamma)}^{(p)}\chi_2^{(\alpha\beta\gamma)}$$

$$\bar{\epsilon}_{33} = \frac{1}{V}\sum_{p=1}^{M}\sum_{\alpha,\ \beta,\ \gamma=1}^{2} v_{(\alpha\beta\gamma)}^{(p)}\psi_2^{(\alpha\beta\gamma)}$$

where $V = H(h_1 + h_2)(l_1 + l_2)$, and $v_{(\alpha\beta\gamma)}^{(p)} = d_\alpha^{(p)} h_\beta l_\gamma$ being the volume of subcell (α, β, $\gamma = 1, 2$).

In a plane strain loading situation these far field average normal strains $\bar{\epsilon}_{22}$ and $\bar{\epsilon}_{33}$ vanish. Under generalized plane strain conditions, on the other hand, these far field normal strains are not known in advance. In this situation, however, the average far field normal stresses are zero. The latter are given by

$$\bar{\sigma}_{22} = \frac{1}{V}\sum_{p=1}^{M}\sum_{\alpha,\ \beta,\ \gamma=1}^{2} v_{(\alpha\beta\gamma)}^{(p)} S_{22(0,\ 0,\ 0)}^{(\alpha\beta\gamma)}$$

$$\bar{\sigma}_{33} = \frac{1}{V}\sum_{p=1}^{M}\sum_{\alpha,\ \beta,\ \gamma=1}^{2} v_{(\alpha\beta\gamma)}^{(p)} S_{33(0,\ 0,\ 0)}^{(\alpha\beta\gamma)}$$

where $S_{22(0,0,0)}^{(\alpha\beta\gamma)}$ and $S_{33(0,0,0)}^{(\alpha\beta\gamma)}$ denote the average normal stresses in the subcell in the 2- and 3-direction, respectively (their explicit expressions are given in the sequel).

Thus, either

$$\bar{\epsilon}_{22} = \bar{\epsilon}_{33} = 0 \tag{24}$$

or

$$\bar{\sigma}_{22} = \bar{\sigma}_{33} = 0 \tag{25}$$

must be satisfied, depending on whether plane strain or generalized plane strain conditions hold.

5.2. Thermal analysis

Like the displacement field given above, the derivation from T_0 of the temperature distribution in the subcell ($\alpha\beta\gamma$) of the generic cell (p, q, r) is represented by

$$T^{(\alpha\beta\gamma)} = T_1^{(\alpha\beta\gamma)} + \bar{x}_1^{(\alpha)} T_2^{(\alpha\beta\gamma)} + \tfrac{1}{2}(3\bar{x}_1^{(\alpha)2} - \tfrac{1}{4}d_\alpha^{(p)2}) T_3^{(\alpha\beta\gamma)} + \tfrac{1}{2}(3\bar{x}_2^{(\beta)2} - \tfrac{1}{4}h_\beta^2) T_4^{(\alpha\beta\gamma)} + \tfrac{1}{2}(3\bar{x}_3^{(\gamma)2} - \tfrac{1}{4}l_\gamma^2) T_5^{(\alpha\beta\gamma)} \tag{26}$$

where $T_1^{(\alpha\beta\gamma)}$, which is the temperature at the center of the subcell (i.e. the average temperature over the subcell), and $T_i^{(\alpha\beta\gamma)}$ ($i = 2,\ldots,5$) are unknown coefficients which are determined from the satisfaction of the govern equations (2)–(6) in the subcells, and the continuity and boundary conditions of Section 4.

5.3. Diffusion analysis

The deviation from C_0 of the moisture concentration distribution in the subcell ($\alpha\beta\gamma$) is represented by

$$C^{\alpha\beta\gamma)} = C_1^{(\alpha\beta\gamma)} + \bar{x}_1^{(\alpha)} C_2^{(\alpha\beta\gamma)} + \tfrac{1}{2}(3\bar{x}_1^{(\alpha)2} - \tfrac{1}{4}d_\alpha^{(p)2}) C_3^{(\alpha\beta\gamma)} + \tfrac{1}{2}(3\bar{x}_2^{(\beta)2} - \tfrac{1}{4}h_\beta^2) C_4^{(\alpha\beta\gamma)} + \tfrac{1}{2}(3\bar{x}_3^{(\gamma)2} - \tfrac{1}{4}l_\gamma^2) C_5^{(\alpha\beta\gamma)} \tag{27}$$

where $C_1^{(\alpha\beta\gamma)}$, which is the moisture concentration at the center of the subcell (i.e. the average moisture concentration over the subcell), and $C_i^{(\alpha\beta\gamma)}$ ($i = 2,\ldots,5$) are unknown coefficients which are determined from the satisfaction of the coupled equations (2)–(6) in the subcells, together with the continuity and boundary conditions in Section 4.

6. Volumetric analysis

6.1. Average field variables

The present approximate analysis is based on the satisfaction of the mechanical equilibrium equation (2), the energy equation (5), the coupled diffusion equation (6), and the continuity and boundary conditions, specified in Section 4, in an average sense rather than in a pointwise manner.

To this end let us define the following stress quantities

$$S^{(\alpha\beta\gamma)}_{ij(l,\,m,\,n)} = \frac{1}{v^{(p)}_{(\alpha\beta\gamma)}} \int_{-d_\alpha^{(p)}/2}^{d_\alpha^{(p)}/2} \int_{-h_\beta/2}^{h_\beta/2} \int_{-l_\gamma/2}^{l_\gamma/2} (\bar{x}_1^{(\alpha)})^l (\bar{x}_2^{(\beta)})^m (\bar{x}_3^{(\gamma)})^n \sigma_{ij}^{(\alpha\beta\gamma)}\, \mathrm{d}\bar{x}_1^{(\alpha)}\, \mathrm{d}\bar{x}_2^{(\beta)}\, \mathrm{d}\bar{x}_3^{(\gamma)} \tag{28}$$

In particular, the zero-order quantities $S^{(\alpha\beta\gamma)}_{ij(0,0,0)}$ represent the average stresses in the subcell. By using constitutive relation, Eq. (1), and expansions (21)–(23), (26) and (27), the resulting non-vanishing zero-, first- and second-order stress quantities are given in Appendix A.

Similarly, let us define the heat flux and moisture flux quantities

$$Q^{(\alpha\beta\gamma)}_{i(l,\,m,\,n)} = \frac{1}{v^{(p)}_{(\alpha\beta\gamma)}} \int_{-d_\alpha^{(p)}/2}^{d_\alpha^{(p)}/2} \int_{-h_\beta/2}^{h_\beta/2} \int_{-l_\gamma/2}^{l_\gamma/2} (\bar{x}_1^{(\alpha)})^l (\bar{x}_2^{(\beta)})^m (\bar{x}_3^{(\gamma)})^n q_i^{(\alpha\beta\gamma)}\, \mathrm{d}\bar{x}_1^{(\alpha)}\, \mathrm{d}\bar{x}_2^{(\beta)}\, \mathrm{d}\bar{x}_3^{(\gamma)} \tag{29}$$

$$F^{(\alpha\beta\gamma)}_{i(l,\,m,\,n)} = \frac{1}{v^{(p)}_{(\alpha\beta\gamma)}} \int_{-d_\alpha^{(p)}/2}^{d_\alpha^{(p)}/2} \int_{-h_\beta/2}^{h_\beta/2} \int_{-l_\gamma/2}^{l_\gamma/2} (\bar{x}_1^{(\alpha)})^l (\bar{x}_2^{(\beta)})^m (\bar{x}_3^{(\gamma)})^n f_i^{(\alpha\beta\gamma)}\, \mathrm{d}\bar{x}_1^{(\alpha)}\, \mathrm{d}\bar{x}_2^{(\beta)}\, \mathrm{d}\bar{x}_3^{(\gamma)} \tag{30}$$

By using constitutive relations (3) and (4), and the field expansions (21)–(23), (26) and (27), the zero- and first-order heat and moisture flux quantities can be evaluated. The resulting explicit expressions are given in Appendix A.

6.2. Volumetric stress equilibrium equations

The volumetric equilibrium equations are based on the satisfaction of the zeroth, first and second moments of the equilibrium equation (2). To this end, let us multiply Eqs. (2) by $(\bar{x}_1^{(\alpha)})^l (\bar{x}_2^{(\beta)})^m (\bar{x}_3^{(\gamma)})^n$, where $l, m, n = 0$, 1, or 2 with $l+m+n \le 2$. Integrating the resulting equations by parts, and using the displacement expansions (21)–(23), we obtain, after some lengthy manipulations, the equations of equilibrium in the subcell region $(\alpha\beta\gamma)$ of the generic cell (p, q, r) in the form

$$I^{(\alpha\beta\gamma)}_{11(0,\,0,\,0)} + J^{(\alpha\beta\gamma)}_{21(0,\,0,\,0)} + K^{(\alpha\beta\gamma)}_{31(0,\,0,\,0)} = 0 \tag{31}$$

$$I^{(\alpha\beta\gamma)}_{11(1,\,0,\,0)} - S^{(\alpha\beta\gamma)}_{11(0,\,0,\,0)} = 0 \tag{32}$$

$$J^{(\alpha\beta\gamma)}_{22(0,\,1,\,0)} - S^{(\alpha\beta\gamma)}_{22(0,\,0,\,0)} = 0 \tag{33}$$

$$K^{(\alpha\beta\gamma)}_{33(0,\,0,\,1)} - S^{(\alpha\beta\gamma)}_{33(0,\,0,\,0)} = 0 \tag{34}$$

$$3I^{(\alpha\beta\gamma)}_{11(0,\,0,\,0)} + J^{(\alpha\beta\gamma)}_{21(0,\,0,\,0)} + K^{(\alpha\beta\gamma)}_{31(0,\,0,\,0)} - 24S^{(\alpha\beta\gamma)}_{11(1,\,0,\,0)}/d^{(p)2}_{\alpha} = 0 \tag{35}$$

$$I^{(\alpha\beta\gamma)}_{11(0,\,0,\,0)} + 3J^{(\alpha\beta\gamma)}_{21(0,\,0,\,0)} + K^{(\alpha\beta\gamma)}_{31(0,\,0,\,0)} - 24S^{(\alpha\beta\gamma)}_{12(0,\,1,\,0)}/h^2_{\beta} = 0 \tag{36}$$

$$I^{(\alpha\beta\gamma)}_{11(0,\,0,\,0)} + J^{(\alpha\beta\gamma)}_{21(0,\,0,\,0)} + 3K^{(\alpha\beta\gamma)}_{31(0,\,0,\,0)} - 24S^{(\alpha\beta\gamma)}_{13(0,\,0,\,1)}/l^2_{\gamma} = 0 \tag{37}$$

where the following interfacial quantities have been defined.

$$I^{(\alpha\beta\gamma)}_{1j(n,\,0,\,0)} = \frac{1}{v^{(p)}_{(\alpha\beta\gamma)}}\left(\frac{d^{(p)}_{\alpha}}{2}\right)^n \int_{-h_\beta/2}^{h_\beta/2}\int_{-l_\gamma/2}^{l_\gamma/2}\left[\sigma^{(\alpha\beta\gamma)}_{1j}\left(\frac{d^{(p)}_{\alpha}}{2}\right) + (-1)^{n+1}\sigma^{(\alpha\beta\gamma)}_{1j}\left(-\frac{d^{(p)}_{\alpha}}{2}\right)\right]\mathrm{d}\bar{x}^{(\beta)}_2\,\mathrm{d}\bar{x}^{(\gamma)}_3 \tag{38}$$

$$J^{(\alpha\beta\gamma)}_{2j(0,\,n,\,0)} = \frac{1}{v^{(p)}_{(\alpha\beta\gamma)}}\left(\frac{h_\beta}{2}\right)^n \int_{-d^{(p)}_{\alpha}/2}^{d^{(p)}_{\alpha}/2}\int_{-l_\gamma/2}^{l_\gamma/2}\left[\sigma^{(\alpha\beta\gamma)}_{2j}\left(\frac{h_\beta}{2}\right) + (-1)^{n+1}\sigma^{(\alpha\beta\gamma)}_{2j}\left(-\frac{h_\beta}{2}\right)\right]\mathrm{d}\bar{x}^{(\alpha)}_1\,\mathrm{d}\bar{x}^{(\gamma)}_3 \tag{39}$$

$$K^{(\alpha\beta\gamma)}_{3j(0,\,0,\,n)} = \frac{1}{v^{(p)}_{(\alpha\beta\gamma)}}\left(\frac{l_\gamma}{2}\right)^n \int_{-d^{(p)}_{\alpha}/2}^{d^{(p)}_{\alpha}/2}\int_{-h_\beta/2}^{h_\beta/2}\left[\sigma^{(\alpha\beta\gamma)}_{3j}\left(\frac{l_\gamma}{2}\right) + (-1)^{n+1}\sigma^{(\alpha\beta\gamma)}_{3j}\left(-\frac{l_\gamma}{2}\right)\right]\mathrm{d}\bar{x}^{(\alpha)}_1\,\mathrm{d}\bar{x}^{(\beta)}_2 \tag{40}$$

Manipulations of Eqs. (31), and (35)–(37) yield explicit expressions for the interfacial stresses $I^{(\alpha\beta\gamma)}_{11(0,0,0)}$, $J^{(\alpha\beta\gamma)}_{21(0,0,0)}$, $K^{(\alpha\beta\gamma)}_{31(0,0,0)}$ in terms of the higher-order stresses. These expressions are given in Appendix B.

6.3. Volumetric energy equations

Similarly, the volumetric energy equations are obtained from the pointwise energy equation (5) by the satisfaction of its zeroth, first and second moments in subcell $(\alpha\beta\gamma)$ of the generic cell (p, q, r). After some lengthy manipulations this provides

$$L^{(\alpha\beta\gamma)}_{1(0,\,0,\,0)} + L^{(\alpha\beta\gamma)}_{2(0,\,0,\,0)} + L^{(\alpha\beta\gamma)}_{3(0,\,0,\,0)} = -[\rho c_{\mathrm{p}}\dot{T}_1 - T_0 d_t \dot{C}_1 + T_0\alpha\dot{S}_{kk(0,\,0,\,0)}]^{(\alpha\beta\gamma)} \tag{41}$$

$$L^{(\alpha\beta\gamma)}_{1(1,\,0,\,0)} - Q^{(\alpha\beta\gamma)}_{1(0,\,0,\,0)} = -\frac{d^{(p)2}_{\alpha}}{12}[\rho c_{\mathrm{p}}\dot{T}_2 - T_0 d_t \dot{C}_2]^{(\alpha\beta\gamma)} - T_0\alpha\dot{S}^{(\alpha\beta\gamma)}_{kk(1,\,0,\,0)} \tag{42}$$

$$\begin{aligned}&\frac{d^{(p)2}_{\alpha}}{4}\left[L_{1(0,\,0,\,0)} + \frac{1}{3}(L_{2(0,\,0,\,0)} + L_{3(0,\,0,\,0)})\right]^{(\alpha\beta\gamma)} - 2Q^{(\alpha\beta\gamma)}_{1(1,\,0,\,0)}\\ &\quad = -\frac{d^{(p)2}_{\alpha}}{12}\left[\rho c_{\mathrm{p}}\left(\dot{T}_1 + \frac{d^{(p)2}_{\alpha}}{10}\dot{T}_3\right) - T_0 d_t\left(\dot{C}_1 + \frac{d^{(p)2}_{\alpha}}{10}\dot{C}_3\right)\right]^{(\alpha\beta\gamma)} - T_0\alpha\dot{S}^{(\alpha\beta\gamma)}_{kk(2,\,0,\,0)}\end{aligned} \tag{43}$$

$$\frac{h_\beta^2}{4}\left[L_{2(0,\,0,\,0)}+\frac{1}{3}(L_{1(0,\,0,\,0)}+L_{3(0,\,0,\,0)})\right]^{(\alpha\beta\gamma)}-2Q^{(\alpha\beta\gamma)}_{2(0,\,1,\,0)}$$
$$=-\frac{h_\beta^2}{12}\left[\rho c_{\mathrm{p}}\left(\dot{T}_1+\frac{h_\beta^2}{10}\dot{T}_4\right)-T_0 d_t\left(\dot{C}_1+\frac{h_\beta^2}{10}\dot{C}_4\right)\right]^{(\alpha\beta\gamma)}-T_0\alpha\dot{S}^{(\alpha\beta\gamma)}_{kk(0,\,2,\,0)} \tag{44}$$

$$\frac{l_\gamma^2}{4}\left[L_{3(0,\,0,\,0)}+\frac{1}{3}(L_{1(0,\,0,\,0)}+L_{2(0,\,0,\,0)})\right]^{(\alpha\beta\gamma)}-2Q^{(\alpha\beta\gamma)}_{3(0,\,0,\,1)}$$
$$=-\frac{l_\gamma^2}{12}\left[\rho c_{\mathrm{p}}\left(\dot{T}_1+\frac{l_\gamma^2}{10}\dot{T}_5\right)-T_0 d_t\left(\dot{C}_1+\frac{l_\gamma^2}{10}\dot{C}_5\right)\right]^{(\alpha\beta\gamma)}-T_0\alpha\dot{S}^{(\alpha\beta\gamma)}_{kk(0,\,0,\,2)} \tag{45}$$

In these equations a dot denotes time derivative, and the interfacial heat flux quantities $L^{(\alpha\beta\gamma)}_{i(l,\,m,\,n)}$ are defined below.

$$L^{(\alpha\beta\gamma)}_{1(n,\,0,\,0)}=\frac{1}{v^{(p)}_{(\alpha\beta\gamma)}}\left(\frac{d^{(p)}_\alpha}{2}\right)^n\int_{-h_\beta/2}^{h_\beta/2}\int_{-l_\gamma/2}^{l_\gamma/2}\left[q_1^{(\alpha\beta\gamma)}\left(\frac{d^{(p)}_\alpha}{2}\right)+(-1)^{n+1}q_1^{(\alpha\beta\gamma)}\left(-\frac{d^{(p)}_\alpha}{2}\right)\right]\mathrm{d}\bar{x}_2^{(\beta)}\,\mathrm{d}\bar{x}_3^{(\gamma)} \tag{46}$$

$$L^{(\alpha\beta\gamma)}_{2(0,\,n,\,0)}=\frac{1}{v^{(p)}_{(\alpha\beta\gamma)}}\left(\frac{h_\beta}{2}\right)^n\int_{-d^{(p)}_\alpha/2}^{d^{(p)}_\alpha/2}\int_{-l_\gamma/2}^{l_\gamma/2}\left[q_2^{(\alpha\beta\gamma)}\left(\frac{h_\beta}{2}\right)+(-1)^{n+1}q_2^{(\alpha\beta\gamma)}\left(-\frac{h_\beta}{2}\right)\right]\mathrm{d}\bar{x}_1^{(\alpha)}\,\mathrm{d}\bar{x}_3^{(\gamma)} \tag{47}$$

$$L^{(\alpha\beta\gamma)}_{3(0,\,0,\,n)}=\frac{1}{v^{(p)}_{(\alpha\beta\gamma)}}\left(\frac{l_\gamma}{2}\right)^n\int_{-d^{(p)}_\alpha/2}^{d^{(p)}_\alpha/2}\int_{-h_\beta/2}^{h_\beta/2}\left[q_3^{(\alpha\beta\gamma)}\left(\frac{l_\gamma}{2}\right)+(-1)^{n+1}q_3^{(\alpha\beta\gamma)}\left(-\frac{l_\gamma}{2}\right)\right]\mathrm{d}\bar{x}_1^{(\alpha)}\,\mathrm{d}\bar{x}_2^{(\beta)} \tag{48}$$

Manipulation of the four equations (41), and (43)–(45) yield explicit expressions for the above interfacial heat flux quantities $L^{(\alpha\beta\gamma)}_{1(0,0,0)}$, $L^{(\alpha\beta\gamma)}_{2(0,0,0)}$, $L^{(\alpha\beta\gamma)}_{3(0,0,0)}$ which are given in Appendix B.

6.4. Volumetric diffusion equations

The same operations on the coupled diffusion equation (6) yield five volumetric equations which are given in the following

$$M^{(\alpha\beta\gamma)}_{1(0,\,0,\,0)}+M^{(\alpha\beta\gamma)}_{2(0,\,0,\,0)}+M^{(\alpha\beta\gamma)}_{3(0,\,0,\,0)}=-\dot{C}_1^{(\alpha\beta\gamma)} \tag{49}$$

$$M^{(\alpha\beta\gamma)}_{1(1,\,0,\,0)}-F^{(\alpha\beta\gamma)}_{1(0,\,0,\,0)}=-\frac{d^{(p)2}_\alpha}{12}\dot{C}_2^{(\alpha\beta\gamma)} \tag{50}$$

$$3M^{(\alpha\beta\gamma)}_{1(0,\,0,\,0)}+M^{(\alpha\beta\gamma)}_{2(0,\,0,\,0)}+M^{(\alpha\beta\gamma)}_{3(0,\,0,\,0)}-24F^{(\alpha\beta\gamma)}_{1(1,\,0,\,0)}/d^{(p)2}_\alpha=-\left[\dot{C}_1+\frac{d^{(p)2}_\alpha}{10}\dot{C}_3\right]^{(\alpha\beta\gamma)} \tag{51}$$

$$M^{(\alpha\beta\gamma)}_{1(0,\,0,\,0)}+3M^{(\alpha\beta\gamma)}_{2(0,\,0,\,0)}+M^{(\alpha\beta\gamma)}_{3(0,\,0,\,0)}-24F^{(\alpha\beta\gamma)}_{2(0,\,1,\,0)}/h_\beta^2=-\left[\dot{C}_1+\frac{h_\beta^2}{10}\dot{C}_4\right]^{(\alpha\beta\gamma)} \tag{52}$$

$$M^{(\alpha\beta\gamma)}_{1(0,\,0,\,0)} + M^{(\alpha\beta\gamma)}_{2(0,\,0,\,0)} + 3M^{(\alpha\beta\gamma)}_{3(0,\,0,\,0)} - 24F^{(\alpha\beta\gamma)}_{3(0,\,0,\,1)}/l_\gamma^2 = -\left[\dot{C}_1 + \frac{l_\gamma^2}{10}\dot{C}_5\right]^{(\alpha\beta\gamma)} \tag{53}$$

The interfacial moisture flux $M^{(\alpha\beta\gamma)}_{i(l,\,m,\,n)}$ are defined just like the interfacial heat flux quantities in Eqs. (46)–(48), but with q_i replaced by f_i. Manipulation of the four relations (49), (51)–(53) yields explicit expressions for the interfacial moisture fluxes $M^{(\alpha\beta\gamma)}_{1(0,0,0)}$, $M^{(\alpha\beta\gamma)}_{2(0,0,0)}$, $M^{(\alpha\beta\gamma)}_{3(0,0,0)}$ which are given in Appendix B.

7. The governing equations

The governing coupled equations of the hygrothermoelastic multiphase composite are based on the previously derived zeroth, first and second moments of the equilibrium, energy and diffusion equations, as well as the satisfaction of the host of interfacial continuity and boundary conditions are described in Section 4.

7.1. The governing mechanical equations

In Aboudi et al. (1994, 1995) the governing uncoupled mechanical equations were established. In the present coupled case the combined effects of temperature and moisture must be included. Following the same methodology, these equations can be presented in the following form

$$\left[d_1\dot{I}^{(1\beta\gamma)}_{11(0,\,0,\,0)} + \frac{d_2}{2}\dot{I}^{(2\beta\gamma)}_{11(0,\,0,\,0)} - \dot{I}^{(2\beta\gamma)}_{11(1,\,0,\,0)}\right]^{(p,\,q,\,r)} + \left[\frac{d_2}{2}\dot{I}^{(2\beta\gamma)}_{11(0,\,0,\,0)} + \dot{I}^{(2\beta\gamma)}_{11(1,\,0,\,0)}\right]^{(p-1,\,q,\,r)} = 0 \tag{54}$$

$$-\left[\frac{d_2}{4}\dot{I}^{(2\beta\gamma)}_{11(0,\,0,\,0)} + \dot{I}^{(1\beta\gamma)}_{11(1,\,0,\,0)} - \frac{1}{2}\dot{I}^{(2\beta\gamma)}_{11(1,\,0,\,0)}\right]^{(p,\,q,\,r)} + \left[\frac{d_2}{4}\dot{I}^{(2\beta\gamma)}_{11(0,\,0,\,0)} + \frac{1}{2}\dot{I}^{(2\beta\gamma)}_{11(1,\,0,\,0)}\right]^{(p-1,\,q,\,r)} = 0 \tag{55}$$

$$h_1\dot{J}^{(\alpha1\gamma)}_{21(0,\,0,\,0)} + h_2\dot{J}^{(\alpha2\gamma)}_{21(0,\,1,\,0)}]^{(p,\,q,\,r)} = 0 \tag{56}$$

$$[\dot{J}^{(\alpha1\gamma)}_{22(0,\,1,\,0)} - \dot{J}^{(\alpha2\gamma)}_{22(0,\,1,\,0)}]^{(p,\,q,\,r)} = 0 \tag{57}$$

$$[l_1\dot{K}^{(\alpha\beta1)}_{31(0,\,0,\,0)} + l_2\dot{K}^{(\alpha\beta2)}_{31(0,\,0,\,0)}]^{(p,\,q,\,r)} = 0 \tag{58}$$

$$[\dot{K}^{(\alpha\beta1)}_{33(0,\,0,\,1)} - \dot{K}^{(\alpha\beta2)}_{33(0,\,0,\,1)}]^{(p,\,q,\,r)} = 0 \tag{59}$$

Furthermore, the continuity conditions of the displacements in the 1-direction at each subcell interface, Eqs. (9), yield the following conditions for the pth cell

$$\left[\dot{w}_1^{(1\beta\gamma)} + \frac{d_1}{2}\dot{\phi}_1^{(1\beta\gamma)} + \frac{d_1^2}{4}\dot{U}_1^{(1\beta\gamma)}\right]^{(p,\,q,\,r)} = \left[\dot{w}_1^{(2\beta\gamma)} - \frac{d_2}{2}\dot{\phi}_1^{(2\beta\gamma)} + \frac{d_2^2}{4}\dot{U}_1^{(2\beta\gamma)}\right]^{(p,\,q,\,r)} \tag{60}$$

$$\left[\dot{w}_1^{(\alpha1\gamma)} + \frac{h_1^2}{4}\dot{V}_1^{(\alpha2\gamma)}\right]^{(p,\,q,\,r)} = \left[\dot{w}_1^{(\alpha2\gamma)} + \frac{h_2^2}{4}\dot{V}_1^{(\alpha2\gamma)}\right]^{(p,\,q,\,r)} \tag{61}$$

$$\left[\dot{w}_1^{(\alpha\beta 1)} + \frac{l_1^2}{4}\dot{W}_1^{(\alpha\beta 1)}\right]^{(p,\,q,\,r)} = \left[\dot{w}_1^{(\alpha\beta 2)} + \frac{l_2^2}{4}\dot{W}_1^{(\alpha\beta 1)}\right]^{(p,\,q,\,r)} \tag{62}$$

Continuity of the displacements in the 2- and 3-directions, yield, respectively,

$$[h_1\dot{\chi}_2^{(\alpha 1\gamma)} + h_2\dot{\chi}_2^{(\alpha 2\gamma)}]^{(p,\,q,\,r)} - (h_1 + h_2)\dot{\bar{\epsilon}}_{22} = 0 \tag{63}$$

$$[l_1\dot{\psi}_3^{(\alpha\beta 1)} + l_2\dot{\psi}_3^{(\alpha\beta 2)}]^{(p,\,q,\,r)} - (l_1 + l_2)\dot{\bar{\epsilon}}_{33} = 0 \tag{64}$$

The continuity of displacement between neighboring cells in the 1-direction, Eqs. (10), on the other hand provides

$$\left[\dot{w}_1^{(1\beta\gamma)} - \frac{d_1}{2}\dot{\phi}_1^{(1\beta\gamma)} + \frac{d_1^2}{4}\dot{U}_1^{(1\beta\gamma)}\right]^{(p+1,\,q,\,r)} = \left[\dot{w}_1^{(2\beta\gamma)} + \frac{d_2}{2}\dot{\phi}_1^{(2\beta\gamma)} + \frac{d_2^2}{4}\dot{U}_1^{(2\beta\gamma)}\right]^{(p,\,q,\,r)} \tag{65}$$

These relations fulfill all the necessary moments of equilibrium, continuity and boundary requirements. They form together with the rate of Eq. (31) a system of 56 M linear algebraic equations in the time rate of the microvariables that appear in Eqs. (21)–(23), (26) and (27). An additional two relations result from (24) or (25), depending on whether plane strain or generalized plane strain conditions hold.

7.2. The governing energy equations

By following the same methodology in establishing the governing equations in the mechanical case, it can be shown that the satisfaction of the moments of the energy equations together with the associated interfacial and boundary conditions, yields after some manipulations, the following set of equations

$$\left[d_1 L_{1(0,\,0,\,0)}^{(1\beta\gamma)} + \frac{d_2}{2}L_{1(0,\,0,\,0)}^{(2\beta\gamma)} - L_{1(1,\,0,\,0)}^{(2\beta\gamma)}\right]^{(p,\,q,\,r)} + \left[\frac{d_2}{2}L_{1(0,\,0,\,0)}^{(2\beta\gamma)} + L_{1(1,\,0,\,0)}^{(2\beta\gamma)}\right]^{(p-1,\,q,\,r)} = 0 \tag{66}$$

$$-\left[\frac{d_2}{4}L_{1(0,\,0,\,0)}^{(2\beta\gamma)} + L_{1(1,\,0,\,0)}^{(1\beta\gamma)} - \frac{1}{2}L_{1(1,\,0,\,0)}^{(2\beta\gamma)}\right]^{(p,\,q,\,r)} + \left[\frac{d_2}{4}L_{1(0,\,0,\,0)}^{(2\beta\gamma)} + \frac{1}{2}L_{1(1,\,0,\,0)}^{(2\beta\gamma)}\right]^{(p-1,\,q,\,r)} = 0 \tag{67}$$

$$[h_1 L_{2(0,\,0,\,0)}^{(\alpha 1\gamma)} + h_2 L_{2(0,\,0,\,0)}^{(\alpha 2\gamma)}]^{(p,\,q,\,r)} = 0 \tag{68}$$

$$[l_1 L_{3(0,\,0,\,0)}^{(\alpha\beta 1)} + l_2 L_{3(0,\,0,\,0)}^{(\alpha\beta 2)}]^{(p,\,q,\,r)} = 0 \tag{69}$$

Furthermore, the continuity conditions of the temperature at each subcell interface, Eqs. (13), yield the following conditions for the pth cell

$$\left[\dot{T}_1^{(1\beta\gamma)} + \frac{d_1}{2}\dot{T}_2^{(1\beta\gamma)} + \frac{d_1^2}{4}\dot{T}_3^{(1\beta\gamma)}\right]^{(p,\,q,\,r)} = \left[\dot{T}_1^{(2\beta\gamma)} - \frac{d_2}{2}\dot{T}_2^{(2\beta\gamma)} + \frac{d_2^2}{4}\dot{T}_3^{(2\beta\gamma)}\right]^{(p,\,q,\,r)} \tag{70}$$

$$\left[\dot{T}_1^{(\alpha 1\gamma)} + \frac{h_1^2}{4}\dot{T}_4^{(\alpha 2\gamma)}\right]^{(p,\,q,\,r)} = \left[\dot{T}_1^{(\alpha 2\gamma)} + \frac{h_2^2}{4}\dot{T}_4^{(\alpha 2\gamma)}\right]^{(p,\,q,\,r)} \tag{71}$$

$$\left[\dot{T}_1^{(\alpha\beta 1)} + \frac{l_1^2}{4}\dot{T}_5^{(\alpha\beta 1)}\right]^{(p,\,q,\,r)} = \left[\dot{T}_1^{(\alpha\beta 2)} + \frac{l_2^2}{4}\dot{T}_5^{(\alpha\beta 1)}\right]^{(p,\,q,\,r)} \tag{72}$$

The continuity of temperature between neighboring cells in the 1-direction, Eqs. (14) on the other hand, provides

$$\left[\dot{T}_1^{(1\beta\gamma)} - \frac{d_1}{2}\dot{T}_2^{(1\beta\gamma)} + \frac{d_1^2}{4}\dot{T}_3^{(1\beta\gamma)}\right]^{(p+1,\,q,\,r)} = \left[\dot{T}_1^{(2\beta\gamma)} + \frac{d_2}{2}\dot{T}_2^{(2\beta\gamma)} + \frac{d_2^2}{4}\dot{T}_3^{(2\beta\gamma)}\right]^{(p,\,q,\,r)} \tag{73}$$

Relations (66)–(73) together with (41) provide a system of 40 M linear algebraic equations in the rates of the microvariables that appear in Eqs. (21)–(23), (26) and (27).

7.3. The governing coupled diffusion equations

The governing equations that represent the diffusion equations are derived in a similar form as the energy equations. Thus, in Eqs. (66)–(69) we replace everywhere $L_{i(l,\,m,\,n)}^{(\alpha\beta\gamma)}$ by $M_{i(l,\,m,\,n)}^{(\alpha\beta\gamma)}$, and in Eqs. (70)–(73) we replace $T_i^{(\alpha\beta\gamma)}$ by $C_i^{(\alpha\beta\gamma)}$. Here too we obtain together with Eq. (49) another linear system of 40 M relations in the time rate of microvariables that appear in Eqs. (21)–(23), (26) and (27).

7.4. Summary of the governing equations

In summary, altogether we have a linear system of 136 M + 2 algebraic equations which govern the rates of the mechanical, temperature and moisture concentration microvariables in subcell $(\alpha\beta\gamma)$ that appear in expansions (21)–(25), (26), (27) and the two far field strain rates $\dot{\bar{\epsilon}}_{22}$, $\dot{\bar{\epsilon}}_{33}$. It should be noted that these equations hold for an arbitrary pth cell in the interior of the composite (i.e. $p = 2,\ldots,M-1$). For the boundary cells (i.e. $p = 1$ and M), most of these relations also hold, with the exception of the interfacial continuity conditions between adjacent cells [e.g. Eqs. (54) and (65)] which must be replaced by the specified boundary conditions.

For a composite that consists of M generic cells, the final system of 136 M + 2 equations can be symbolically represented below

$$\mathbf{A}\dot{\mathbf{U}} = \mathbf{G} \tag{74}$$

where the structural stiffness matrix $\mathbf{A}$ contains information on the geometry and the hygrothermoelastic properties of the materials that fill the individual subcells in the M cells of the multiphase composite. The vector $\dot{\mathbf{U}}$ contains the 136 M + 2 unknown microvariable rates in each subcell, and $\dot{\bar{\epsilon}}_{22}$, $\dot{\bar{\epsilon}}_{33}$, i.e.,

$$\dot{\mathbf{U}} = (\dot{\mathbf{U}}_1^{(111)}, \ldots, \dot{\mathbf{U}}_M^{(222)}, \dot{\bar{\epsilon}}_{22}, \dot{\bar{\epsilon}}_{33}) \tag{75}$$

where $\dot{\mathbf{U}}_p^{(\alpha\beta\gamma)} = (\dot{w}_1, \dot{\phi}_1, \dot{U}_1, \dot{V}_1, \dot{W}_1, \dot{\chi}_2, \dot{\psi}_3, \dot{T}_1, \dot{T}_2, \dot{T}_3, \dot{T}_4, \dot{T}_5, \dot{C}_1, \dot{C}_2, \dot{C}_3, \dot{C}_4, \dot{C}_5)_p^{(\alpha\beta\gamma)}$. The force vector $\mathbf{G}$ contains information on the applied mechanical, thermal and moisture boundary conditions, and also involves the microvariables at the current time t. The solution that establishes the response of the composite is obtained incrementally in time as follows. The system (74) is solved for the rates of the microvariables and far field normal strains at a given time t, wherein $\mathbf{G}$ is evaluated by employing the values of the microvariables that have been already established in the previous time step. From these time rates on can obtain the microvariables themselves and the far field normal strains by a simple Eulerian integration. Once these microvariables have been determined at a given time, we can proceed and compute the hygrothermoelastic field at any point of the multiphase composite at this time. This procedure is continued to the next time step.

8. Applications

In this section results are given that show the effect of coupling between temperature, moisture and deformation. Sih et al. (1986) provide material parameters for a quasi-isotropic graphite/epoxy (T300/5208) laminate that is subjected to a sudden moisture rise such that the relative humidity changes from 0 to 75% at temperature $T_0 = 294$ K. The resulting constants established under such circumstances are given in Table 1.

Another set of material parameters were established by Sih et al. (1986) where the quasi-isotropic laminate is subjected to a temperature change from 21 to 61°C at 75% relative humidity. These parameters are given in Table 2. It should be noted that all results that have been generated in this paper at various times t are scaled and shown with respect to the non-dimensional time $\tau = 50tK_1/H^2\rho c_p$, where K_1 has been defined in Appendix A. This implies that different time scales are referred to, depending on whether the material constants in Tables 1 or 2 are used.

8.1. Homogeneous slab

Let us start by exhibiting the response of a homogeneous slab which is initially at temperature $T_0 = 21$°C and moisture concentration of 75%. Its rigidly clamped boundaries $x_1 = 0$ and $x_1 = H$ are subjected to a sudden temperature change from 21 to 61°C at 75% relative humidity. Under such circumstances the analysis should be based on the data given by Table 2. In Fig. 2 the resulting temperature variations across the slab, due to the applied temperature change of $\Delta T_B = 40$°C at the boundaries $x_1 = 0$, H, together with the induced moisture concentration are shown at different non-dimensional times τ. This figure clearly exhibits the strong coupling that exists between the fields.

In Fig. 3 the corresponding average field values are shown against time for plane strain (PS) and generalized plane strain (GPS) conditions. It is clearly seen that the induced moisture concentrations and stresses that result from the imposed temperature at the boundaries are significant. Both Figs. 2 and 3 show that steady state is well approached at $\tau = 20$.

In order to exhibit the strong coupling that exists between temperature, moisture and deformation, one can consider a hypothetical case in which the effect of deformation is neglected. This implies that in the present case of applied temperature of $\Delta T_B = 40$°C on the boundaries of the slab, no mechanical deformation can be induced. This situation is achieved by simply setting that $\alpha = \eta = 0$ in the governing

Table 1
Material constants of T300/5208 graphite/epoxy quasi-isotropic laminate subjected to change in moisture from 0 to 75% relative humidity, at 21°C (Sih et al., 1986)

Property	Value
E (Young's modulus)	64.3 GPa
ν (Poisson's ratio)	0.33
ρ (mass density)	1590 kg/m^3
α (thermal expansion coefficient)	31.3×10^{-6}/K
η (moisture expansion coefficient)	1.669×10^{-4} m^3/kg
c_p (specific heat at constant pressure)	806.461 m^2/s^2 K
L_{11}	3.544×10^{-18} kg s/m^3
L_{12}	9.153×10^{-12} kg/m s
L_{22}	9.453×10^{-5} kg m/s^3
d_c	1862 m^5/kg s^2
d_t	−1373 m^2/s^2 K

Table 2
Material constants of T300/5208 graphite/epoxy quasi-isotropic laminate subjected to a temperature change from 21 to 61°C at 75% relative humidity (backed out from Sih et al., 1986)

Property	Value
E (Young's modulus)	64.3 GPa
ν (Poisson's ratio)	0.33
ρ (mass density)	1590 kg/m^3
α (thermal expansion coefficient)	31.3×10^{-6}/K
η (moisture expansion coefficient)	1.669×10^{-4} m^3/kg
c_p (specific heat at constant pressure)	806.461 m^2/s^2 K
L_{11}	0.8×10^{-11} kg s/m^3
L_{12}	0.236×10^{-4} kg/m s
L_{22}	281 kg m/s^3
d_c	0.4×10^4 m^5/kg s^2
d_t	-0.118×10^4 m^2/s^2 K

field equations (1)–(6). In Fig. 4 the variation of the temperature and the induced moisture across the slab are shown at $\tau = 1$ and 20. By comparing these plots with those shown in Fig. 2 it can be immediately concluded that the effect of coupling is tremendous in the present case of clamped slab surfaces. It also shows that the mechanical deformation strongly accelerates the heat transfer and moisture diffusion within the slab.

It is also possible to generate the hygrothermomechanical field when the boundaries of the slab are kept traction-free while imposing the same thermal boundary conditions on both surfaces, namely the sudden application of $\Delta T_B = 40°C$. The resulting induced stresses in this case are far lower (e.g. $\bar{\sigma}_{11} = -20$ MPa) than those shown in Fig. 3. As a result, the hygrothermal response under this type of mechanical boundary conditions turns out to be very close to that given in the extreme case of the uncoupled mechanical deformation shown in Fig. 4 where all stresses vanish. This implies that one can

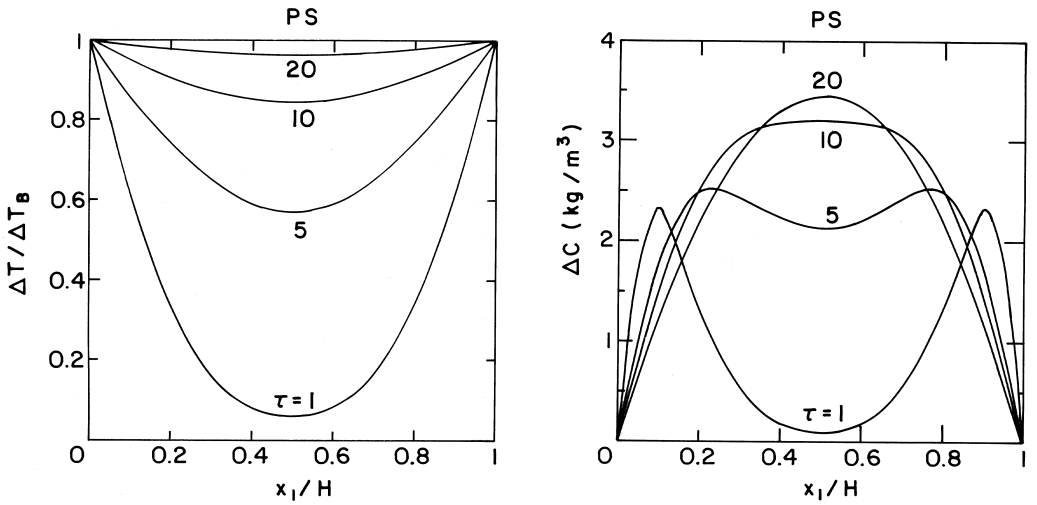

Fig. 2. Temperature and moisture variations across a homogeneous slab whose rigidly clamped boundaries are subjected to a sudden change of temperature under plane strain conditions.

significantly accelerate or decelerate the heat transfer and diffusion process in the slab by controlling the values and signs of the applied mechanical loadings at the boundaries, and the far field normal loads.

As in Figs. 2 and 3, similar results can be generated for a homogeneous slab whose material properties are given by Table 1. The slab is initially at temperature $T_0 = 21°C$ and zero moisture concentration. Its rigidly clamped boundaries are kept at constant temperature $T_0 = 21°C$, while the relative humidity at the surfaces $x_1 = 0$, $x_1 = H$ is changed suddenly from 0 to 75%. The moisture concentration C can be related to the relative humidity by utilizing the relation: $C = \rho M_\infty$, where M_∞ denotes the relative moisture content at equilibrium (i.e. the weight of the absorbed liquid at sufficiently long time divided by the weight of the dry material). For T300/5208, $M_\infty = 1.1\%$ when the relative humidity is 75% (Sih et al., 1986). This implies that the corresponding applied moisture concentration change at the boundaries of the slab $x_1 = 0$, H is $\Delta C_B = 18.48$ kg/m^3.

In Fig. 5, the resulting variation across the slab of the moisture concentration and the induced temperature are shown. The effect of the applied moisture on the induced temperature response is clearly exhibited. In Fig. 6 the resulting average field values in the slab as a function of time are shown

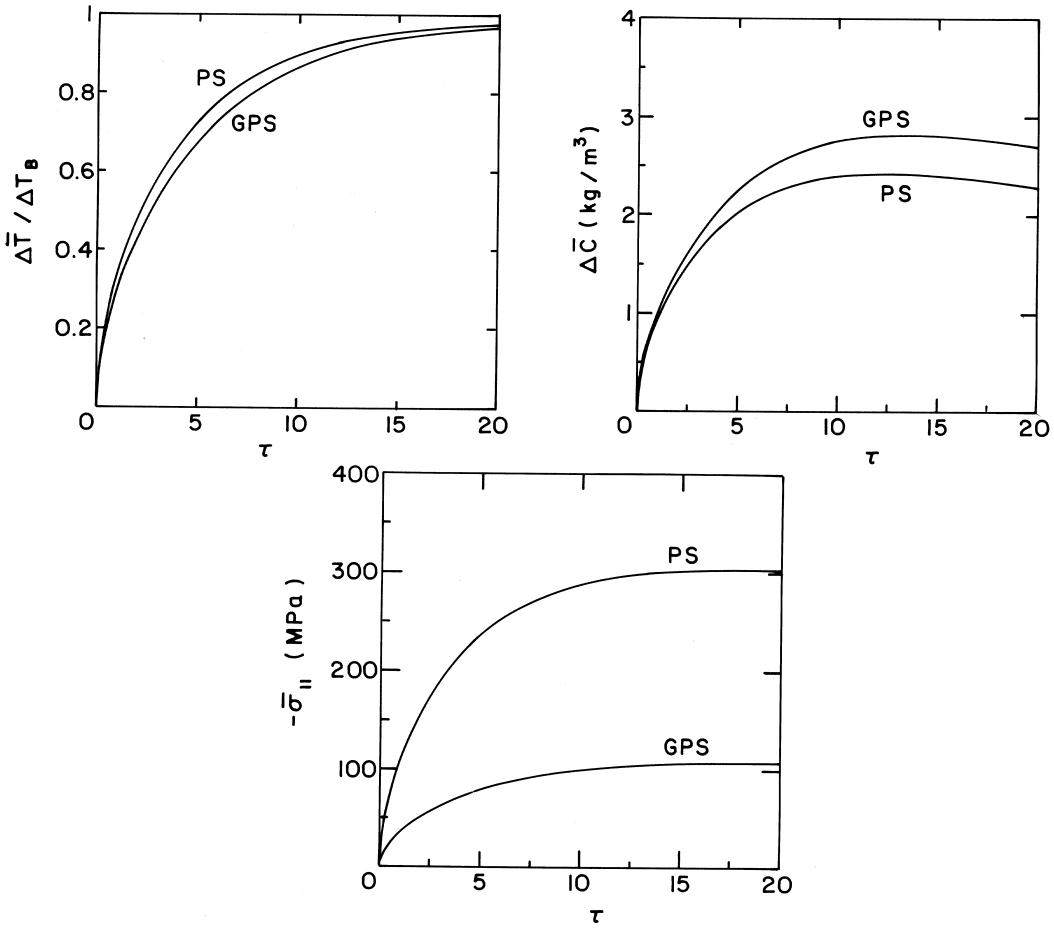

Fig. 3. Time variation of the average temperature, moisture concentration and normal stress of a homogeneous slab subjected to a sudden temperature change at its rigidly clamped boundaries.

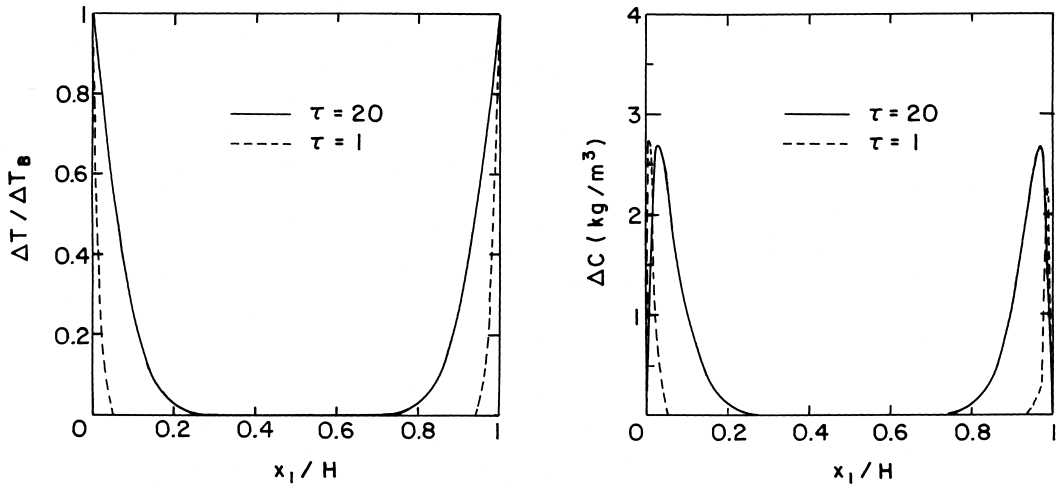

Fig. 4. Temperature and moisture variations across a homogeneous slab whose boundaries are subjected to a sudden change of temperature. The mechanical deformation has been decoupled from the temperature and moisture field.

for plane strain and generalized plane strain conditions. Here too, the strong coupling effects between the fields are clearly displayed. It should be noted that owing to the different time measures associated with Tables 1 and 2, a comparison of Fig. 6 with 3 reveals that the time required for the moisture to approach the steady state is far longer than that required for the heat flow. This is due to the fact that the thermal diffusivity is several orders-of-magnitude greater than the moisture diffusion, as it can be verified from both Tables 1 and 2.

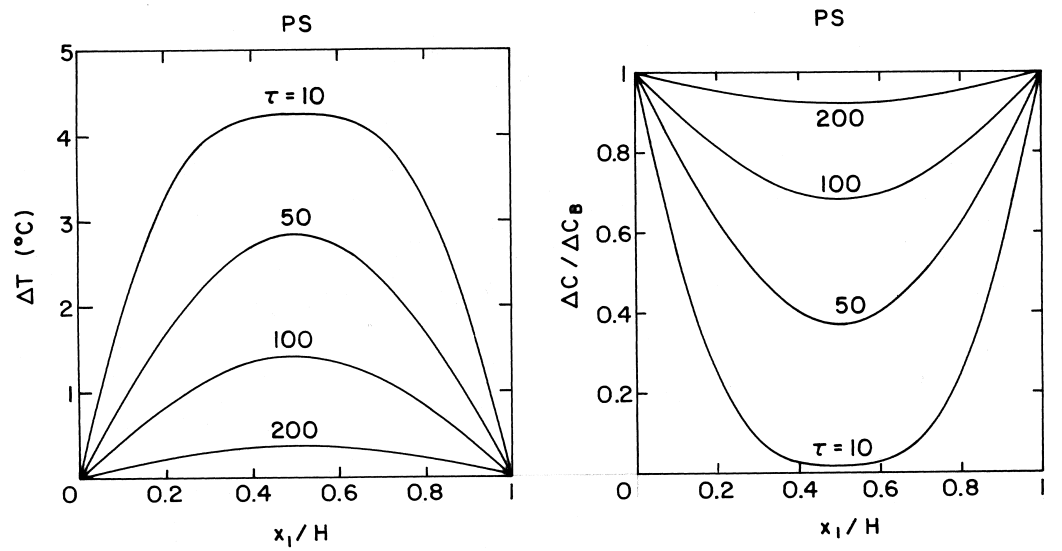

Fig. 5. Temperature and moisture variations across a homogeneous slab whose rigidly clamped boundaries are subjected to a sudden moisture concentration change under plane strain conditions.

Fig. 7 presents the hypothetical situation when the mechanical deformation is decoupled from the temperature and moisture field (obtained by setting $\alpha=\eta=0$). This figure shows the distribution across the thickness of the slab of the moisture concentration and the induced temperature at $\tau=10$ and 200. A comparison with Fig. 5 reveals again the strong effect of the coupling with mechanical deformation which accelerates the diffusion and heat transfer process.

8.2. Porous slab

Consider a slab that is filled by the considered graphite/epoxy (T300/5208) matrix whose properties are described either by Tables 1 or 2. It is assumed that the matrix contains pores with a total porosity of 10%. This situation can be modeled by selecting empty particles in Fig. 1(a), with a volume ratio of 0.1.

Fig. 8 displays the response of the porous slab that is initially at $T = 21°C$ and 75% relative humidity. Its rigidly clamped boundaries $x_1=0$, H are subjected to a sudden change of temperature $\Delta T_B=40°C$ at constant 75% relative humidity. Consequently, the material constants of the

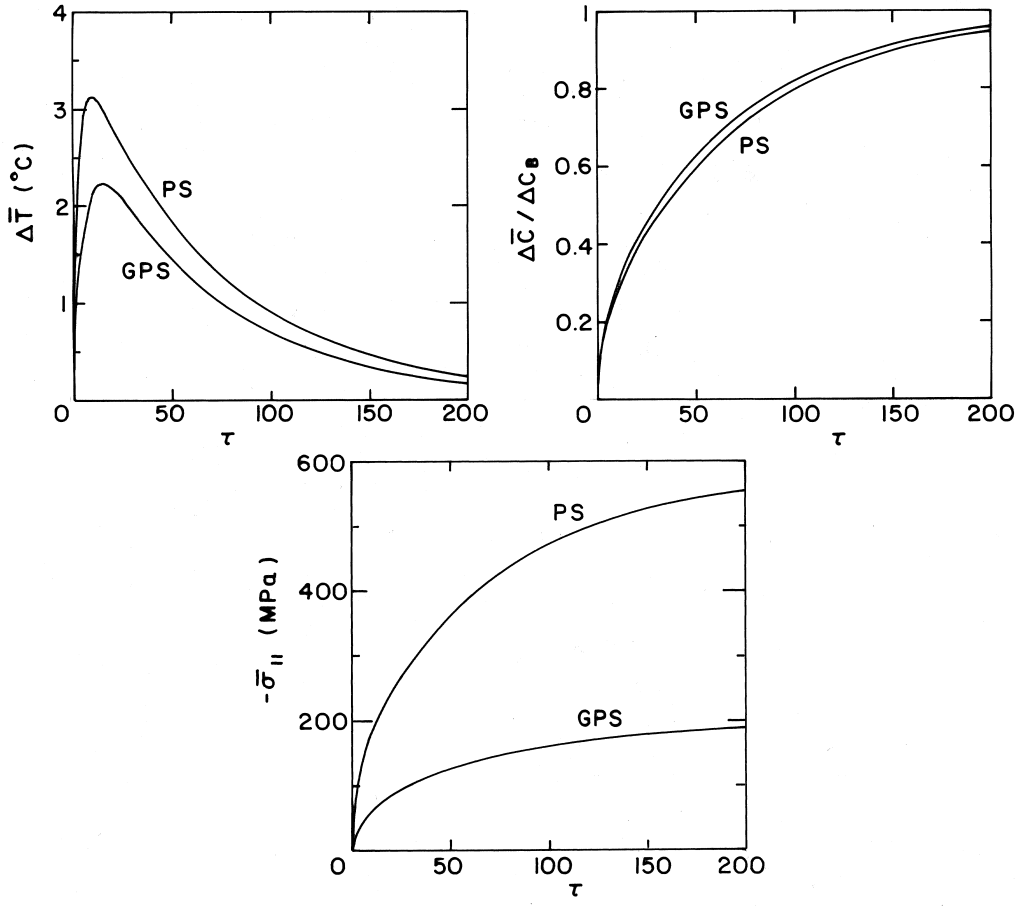

Fig. 6. Time variation of the average temperature, moisture concentration and normal stress of a homogeneous slab subjected to a sudden moisture concentration change at its rigidly clamped boundaries.

homogeneous matrix are described by Table 2. The figure displays the average resulting change in temperature, the induced moisture concentration and normal stress under plane strain and generalized plane strain conditions. Comparison of this figure with the corresponding one of the homogeneous matrix (Fig. 3) shows the strong effect of porosity. As it can be seen from Fig. 3, the steady state situation has been reached at time of about $\tau = 10$. Fig. 8, on the other hand, indicates that due to the existence of porosity the steady state has not been reached as yet, and more time is needed to achieve this situation. In fact due to the existence of the empty pores in the porous slab, its response resembles that of a traction-free homogeneous slab, or, alternatively, a homogeneous slab with uncoupled mechanical deformations. As stated earlier, in both cases the induced stresses are rather low, which result in very slow heat transfer and mass diffusion processes.

The porous material has been modeled by selecting 10 pores that extend uniformly along the thickness of the slab in the x_1-direction, see Fig. 1(a). In Fig. 9 the variation of the induced normal stress $\sigma_{22} = \sigma_{33}$ across the thickness, caused by the sudden application of temperature change of 40°C is shown at time $\tau = 20$ for both plane strain and generalized plane strain conditions. The profiles shown in this figure exhibit abrupt changes while passing from the matrix to the pore regions (where the stresses must vanish). In the generalized plane strain state these profiles attain positive and negative values in order to satisfy the condition that the averages of these normal stresses vanish [see Eq. (25)].

Similar behavior is obtained when a sudden moisture change $\Delta C_B = 18.48$ kg/m^3 is applied on the slab's surfaces $x_1 = 0$, H which are kept rigidly clamped, at a constant temperature $T = 21$°C. Here the constants given by Table 1 are employed to describe the behavior of the homogeneous graphite/epoxy matrix. The response of the porous slab (with 10% porosity) is shown in Fig. 10. This figure should be compared to Fig. 6 of the homogeneous material in order to study the effect of porosity. Here too steady state has not yet been reached whereas it has been approached in the corresponding homogeneous case that is displayed by Fig. 6.

As stated before, Tables 1 and 2 provide the material constants for the sudden application of moisture concentration and temperature, respectively. However, in the absence of other information about the appropriate material constants for applied mechanical deformation, let us utilize these tables

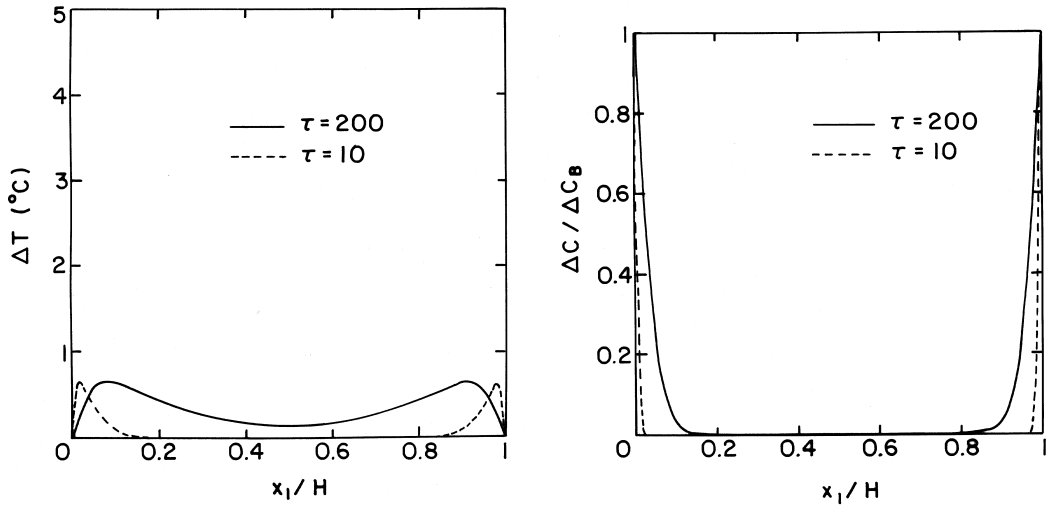

Fig. 7. Temperature and moisture variations across a homogeneous slab whose boundaries are subjected to a sudden change of moisture concentration. The mechanical deformation has been decoupled from the temperature and moisture field.

to study the response of the slab under hydrostatic mechanical loading. To this end consider a mechanical loading in which the following isotropic strain deformation: $\bar{\epsilon}_{11} = \bar{\epsilon}_{22} = \bar{\epsilon}_{33} = 0.01$ has been suddenly applied, while keeping the slab boundaries at $T = T_0 = 21°C$ and $C = C_0 = 18.48$ kg/m^3. The resulting responses are shown in Figs. 11 and 12 when Tables 1 and 2 are, respectively, employed. These two figures (that involve different time scales) present the induced average temperature and moisture changes due to the imposed hydrostatic deformation. Thus, these figures show the effect of coupling that exists between the mechanical deformation and the hygrothermal field.

8.3. Particulate composite slab

Consider a particulate composite that consists of a T300/5208 graphite/epoxy quasi-isotropic laminate filled with Al_2O_3 ceramic particles. The graphite/epoxy hygrothermoelastic matrix is characterized by Table 2, while the thermoelastic properties of the particles are given by Johnson et al. (1994) and presented in Table 3. Suppose that a slab consists of this composite with 10% particles volume ratio.

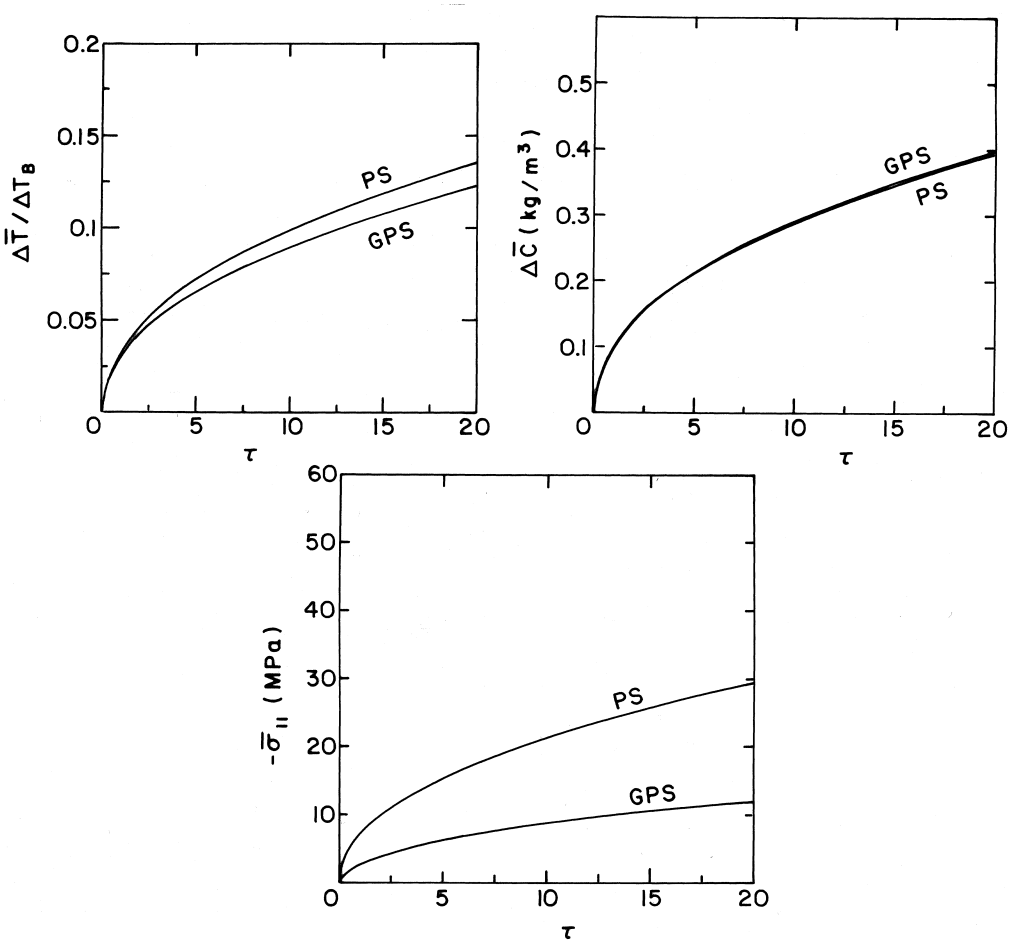

Fig. 8. Time variation of the average temperature, moisture concentration and normal stress of a porous slab subjected to a sudden temperature change at its rigidly clamped boundaries.

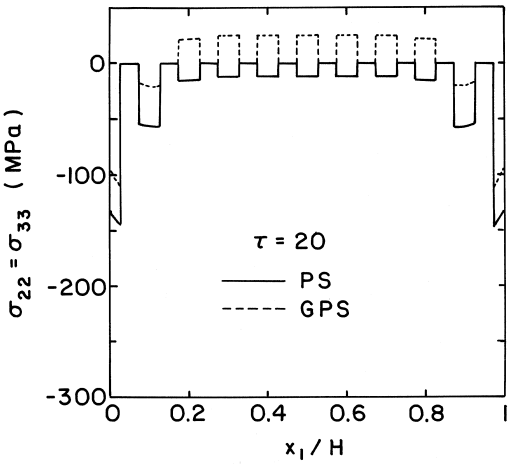

Fig. 9. Normal stress variations across a porous slab whose rigidly clamped boundaries are subjected to a sudden change of temperature at its boundaries.

The slab is initially at temperature $T_0 = 21^\circ C$ and 75% relative humidity. Fig. 13 exhibits the response of this slab whose rigidly clamped surfaces $x_1 = 0$, H are subjected to a sudden change of temperature $\Delta T_B = 40^\circ C$ while the relative humidity is kept at constant. It should be noted that it is assumed (according to Table 3) that no mass diffusion takes place in the ceramic particles, but contrary to the extreme case of empty pores they possess thermoelastic properties and conduct heat. Comparison of this figure with the corresponding one for the porous slab, Fig. 8, shows the effect of the ceramic particles on the particulate composite response. As it can be expected, higher values of the stresses are induced in the present case.

As in the case of the porous material, the particulate composite has been modeled by considering 10 particles which are arranged uniformly in the 1-direction, forming a volume ratio of 0.1. In Fig. 14, the induced normal stresses $\sigma_{22} = \sigma_{33}$ caused by the above temperature change at the boundaries are shown across the thickness of the slab under plane strain and generalized plane strain conditions, at time $\tau = 20$. This figure should be compared with Fig. 9 for the porous case. The non-zero stresses that exist in the particles should be noticed.

Table 3
Material constant of Al_2O_3 alumina (Johnson et al., 1994)

Property	Value
E (Young's modulus)	400 GPa
ν (Poisson's ratio)	0.24
ρ (mass density)	3972 kg/m^3
α (thermal expansion coefficient)	16.32×10^{-6}/K
c_v (specific heat at constant volume)	783 m^2/s^2 K
k (thermal conductivity)	30 W/m K

9. Conclusions

A coupled micro–macromechanical analysis has been developed and implemented to study the response of multiphase composites whose phases behave as hygrothermoelastic materials. The model has been applied to a T300/5208 graphite/epoxy quasi-isotropic matrix, since this is the only material whose material parameters are available. Consequently, it was possible to model a porous material and a particulate composite (in which the ceramic particles were assumed to behave as thermoelastic material). The model provides the temporal and spatial response of a composite slab as well as the effect of coupling between the three fields, when it is subjected to various types of boundary conditions. The present model can be utilized, in particular, to study the effect of the applied stresses on the heat transfer and diffusion process in the composite.

Several generalizations can be considered as follows. (1) The parameters that characterize this type of material are usually moisture and temperature dependent (in particular the moisture diffusivity is strongly temperature sensitive). This effect has not been taken into account due to the unavailability of such information. (2) In the present model perfect bonding has been assumed. It is well known,

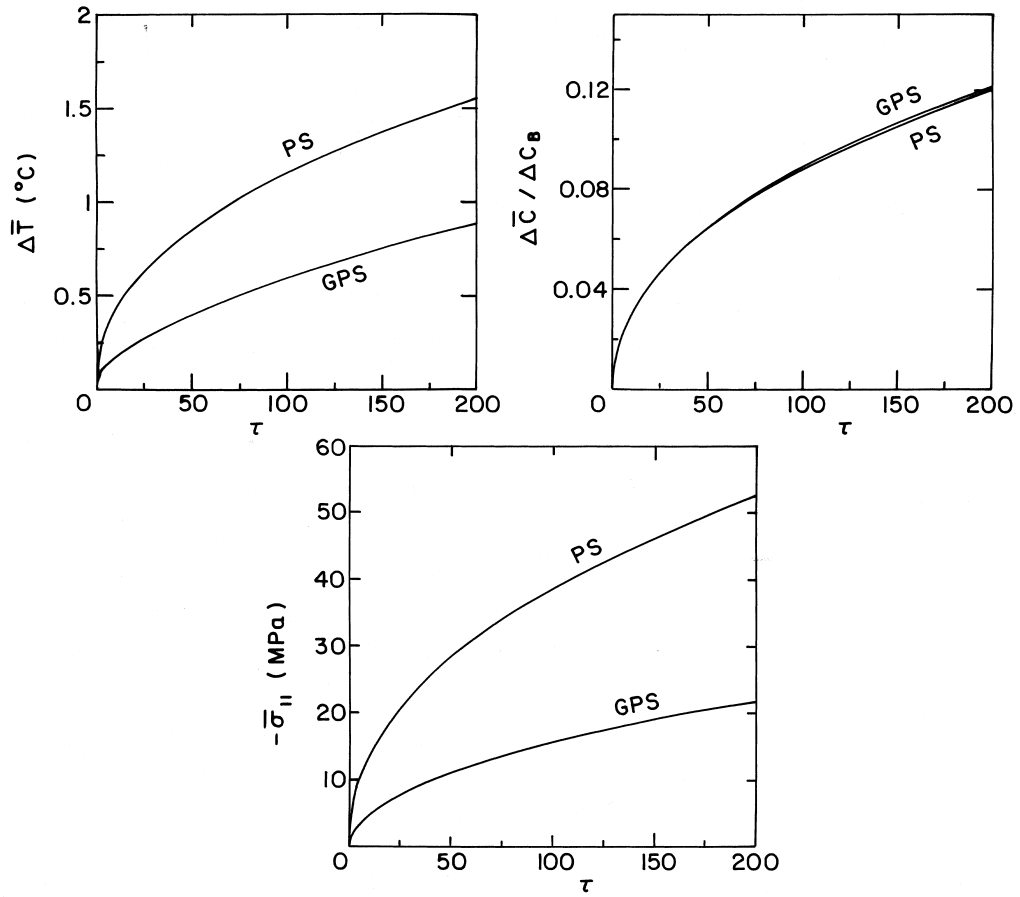

Fig. 10. Time variation of the average temperature, moisture concentration and normal stress of a porous slab subjected to a sudden moisture concentration change at its rigidly clamped boundaries.

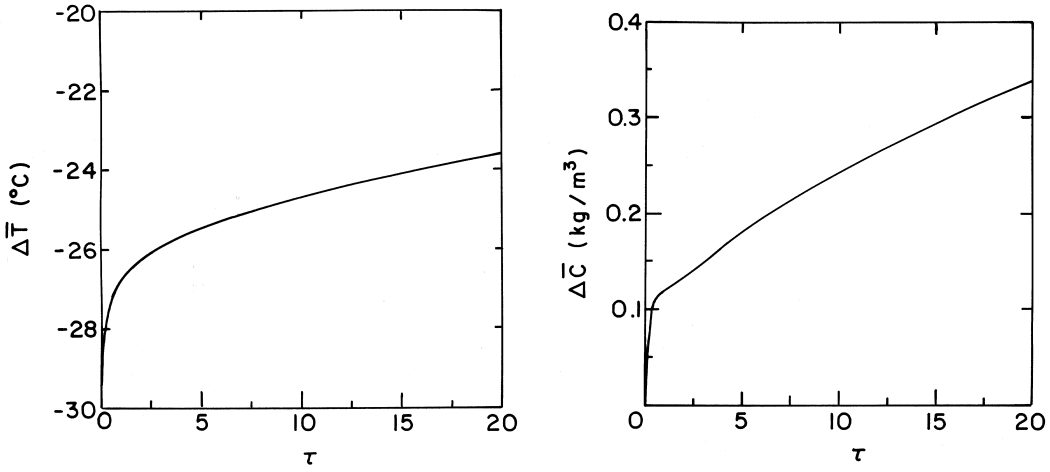

Fig. 11. Time variation of the average temperature and moisture concentration of a porous slab that is subjected to a sudden application of a hydrostatic strain: $\bar{\epsilon}_{11} = \bar{\epsilon}_{22} = \bar{\epsilon}_{33} = 1\%$, while keeping its boundaries at $T = T_0$ and zero moisture. The material parameters of the matrix are characterized by Table 1.

however, that interfacial damage takes place with increase of moisture content in composites. Interfacial damage can be incorporated in the present analysis. (3) Damage also occurs in the form of microcracking. The present approach can be potentially extended to incorporate these effects by utilizing continuum damage mechanics considerations.

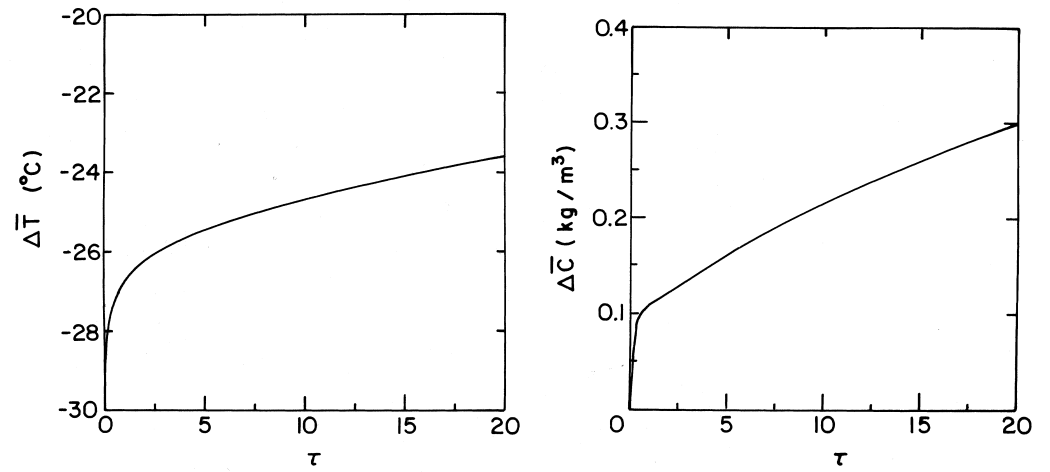

Fig. 12. Time variation of the average temperature and moisture concentration of a porous slab that is subjected to a sudden application of a hydrostatic strain: $\bar{\epsilon}_{11} = \bar{\epsilon}_{22} = \bar{\epsilon}_{33} = 1\%$, while keeping its boundaries at $T = T_0$ and zero moisture. The material parameters of the matrix are characterized by Table 2.

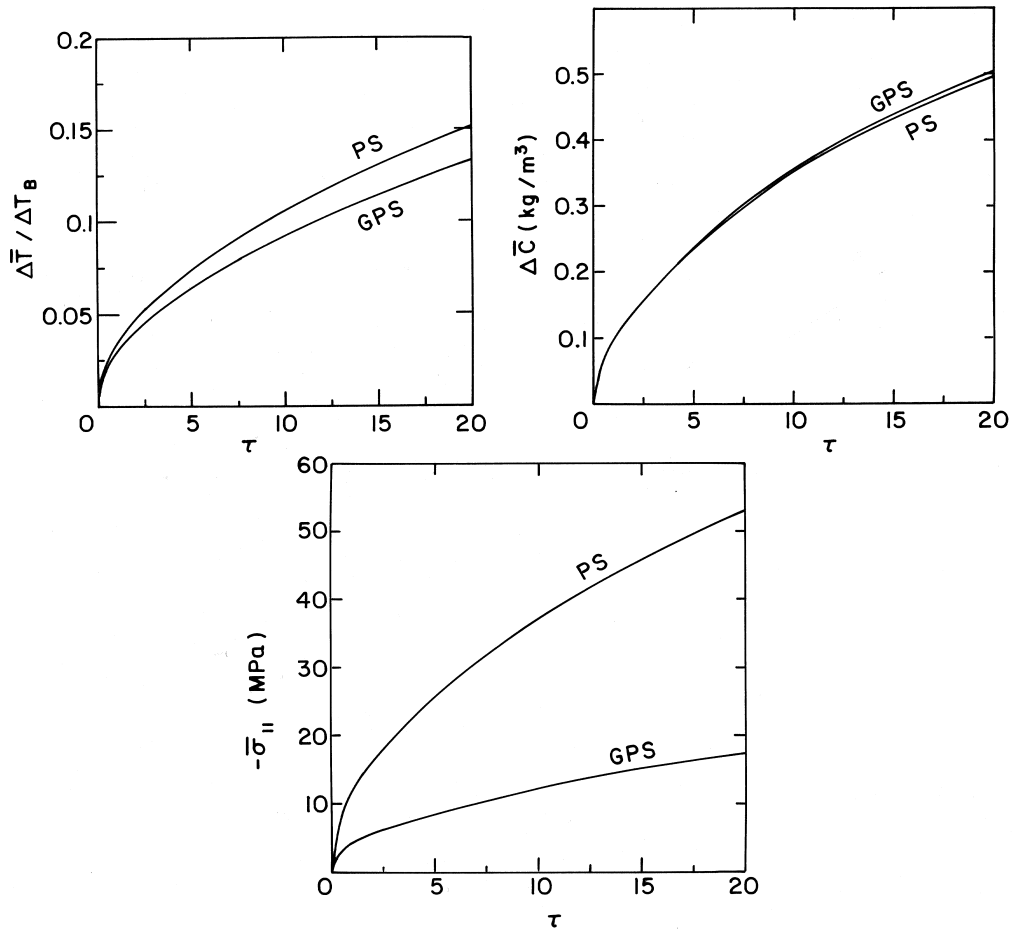

Fig. 13. Time variation of the average temperature, moisture concentration and normal stress of a slab that consists of a particulate material. The slab is subjected to a sudden temperature change at its rigidly clamped boundaries.

Acknowledgements

The first author gratefully acknowledges the support of the Diane and Arthur Belfer chair of Mechanics and Biomechanics. He is also grateful to Prof. Neima Brauner, Tel-Aviv University, for fruitful discussions concerning the diffusion process. Also thanks go to Mr M. Castelli, OAI/NASA-Lewis Research Center, for providing the authors several papers and review articles on hygrothermal effects in composites.

Appendix A

The components of the volumetric stress quantities $S^{(\alpha\beta\gamma)}_{ij(l,\ m}$, $n)$ are given in the following. For simplicity, the superscripts $(\alpha\beta\gamma)$ have been omitted.

$$S_{11(0,\ 0,\ 0)} = (\lambda + 2\mu)\phi_1 + \lambda(\chi_2 + \psi_3) - \Gamma T_1 - \Lambda C_1 \tag{A1}$$

$$S_{22(0,\,0,\,0)} = (\lambda + 2\mu)\chi_2 + \lambda(\phi_1 + \psi_3) - \Gamma T_1 - \Lambda C_1 \tag{A2}$$

$$S_{33(0,\,0,\,0)} = (\lambda + 2\mu)\psi_2 + \lambda(\phi_1 + \chi_3) - \Gamma T_1 - \Lambda C_1 \tag{A3}$$

$$S_{11(1,\,0,\,0)} = \frac{d_\alpha^{(p)2}}{12}[3(\lambda + 2\mu)U_1 - \Gamma T_2 - \Lambda C_2] \tag{A4}$$

$$S_{kk(1,\,0,\,0)} = \frac{d_\alpha^{(p)2}}{4}[(3\lambda + 2\mu)U_1 - \Gamma T_2 - \Lambda C_2] \tag{A5}$$

$$S_{kk(2,\,0,\,0)} = \frac{d_\alpha^{(p)2}}{12}\left[(3\lambda + 2\mu)(\phi_1 + \chi_2 + \psi_3) - 3\Gamma\left(T_1 + \frac{d_\alpha^{(p)2}}{10}T_3\right) - 3\Lambda\left(C_1 + \frac{d_\alpha^{(p)2}}{10}C_3\right)\right] \tag{A6}$$

$$S_{kk(0,\,2,\,0)} = \frac{h_\beta^2}{12}\left[(3\lambda + 2\mu)(\phi_1 + \chi_2 + \psi_3) - 3\Gamma\left(T_1 + \frac{h_\beta^2}{10}T_4\right) - 3\Lambda\left(C_1 + \frac{h_\beta^2}{10}C_4\right)\right] \tag{A7}$$

$$S_{kk(0,\,0,\,2)} = \frac{l_\gamma^2}{12}\left[(3\lambda + 2\mu)(\phi_1 + \chi_2 + \psi_3) - 3\Gamma\left(T_1 + \frac{l_\gamma^2}{10}T_5\right) - 3\Lambda\left(C_1 + \frac{l_\gamma^2}{10}C_5\right)\right] \tag{A8}$$

$$S_{12(0,\,1,\,0)} = \frac{h_\beta^2}{4}\mu V_1 \tag{A9}$$

$$S_{13(0,\,0,\,1)} = \frac{l_\gamma^2}{4}\mu W_1 \tag{A10}$$

where $\Gamma = (3\lambda + 2\mu)\alpha$ and $\Lambda = (3\lambda + 2\mu)\eta$.

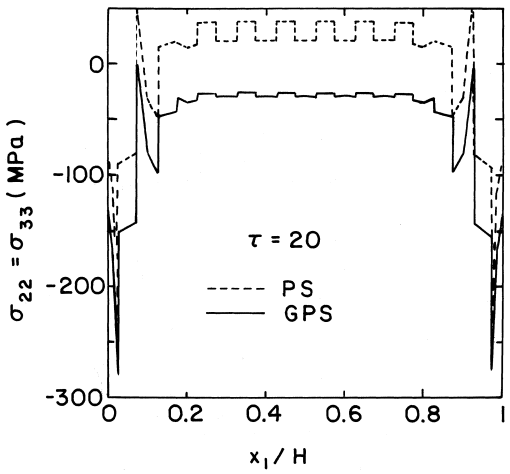

Fig. 14. Normal stress variations across a slab that consists of a particulate material. The slab is subjected to a sudden change of temperature at its rigidly clamped boundaries.

The corresponding expressions for the various zero- and first-order heat moisture flux quantities are as follows

$$Q_{1(0,\,0,\,0)} = -[K_1 T_2 + K_2 C_2 - 3K_3 U_1] \tag{A11}$$

$$Q_{1(1,\,0,\,0)} = -\frac{d_\alpha^{(p)2}}{4}[K_1 T_3 + K_2 C_3] \tag{A12}$$

$$Q_{2(0,\,1,\,0)} = -\frac{h_\beta^2}{4}[K_1 T_4 + K_2 C_4] \tag{A13}$$

$$Q_{3(0,\,0,\,1)} = -\frac{l_\gamma^2}{4}[K_1 T_5 + K_2 C_5] \tag{A14}$$

and

$$F_{1(0,\,0,\,0)} = -[k_1 T_2 + k_2 C_2 - 3k_3 U_1] \tag{A15}$$

$$F_{1(1,\,0,\,0)} = -\frac{d_\alpha^{(p)2}}{4}[k_1 T_3 + k_2 C_3] \tag{A16}$$

$$F_{2(0,\,1,\,0)} = -\frac{h_\beta^2}{4}[k_1 T_4 + k_2 C_4] \tag{A17}$$

$$F_{3(0,\,0,\,1)} = -\frac{l_\gamma^2}{4}[k_1 T_5 + k_2 C_5] \tag{A18}$$

where

$$K_1 = \left(L_{21} d_t + \frac{L_{22}}{T_0} + 3L_{21}\eta\Gamma\right)$$

$$K_2 = L_{21}(d_c + 3\eta\Lambda)$$

$$K_3 = -L_{21}\Lambda$$

$$k_1 = \left(L_{11} d_t + \frac{L_{12}}{T_0} + 3L_{11}\eta\Gamma\right)$$

$$k_2 = L_{11}(d_c + 3\eta\Lambda)$$

$$k_3 = -L_{11}\Lambda$$

Appendix B

The explicit expressions of the interfacial stress quantities are given below. For simplicity, the superscripts $(\alpha\beta\gamma)$ have been omitted in this Appendix

$$I_{11(0,\,0,\,0)} = \frac{12}{d_\alpha^{(p)2}} S_{11(1,\,0,\,0)} \tag{B1}$$

$$J_{21(0,\,0,\,0)} = \frac{12}{h_\beta^2} S_{12(0,\,1,\,0)} \tag{B2}$$

$$K_{31(0,\,0,\,0)} = \frac{12}{l_\gamma^2} S_{13(0,\,0,\,1)} \tag{B3}$$

where the values of these higher-order volumetric stresses have been given in Appendix A. It should be noted the interfacial quantities $I_{11(1,0,0)}$, $J_{22(0,1,0)}$, $K_{33(0,0,1)}$ have already been provided by Eqs. (32)–(34).

The explicit expressions of the interfacial heat flux quantities are given below

$$L_{1(0,\,0,\,0)} = \frac{d_\alpha^{(p)2}}{20}[-\rho c_p \dot{T}_3 + T_0 d_t \dot{C}_3] + \frac{1}{2} T_0 \alpha \left[\dot{S}_{kk(0,\,0,\,0)} - \frac{12}{d_\alpha^{(p)2}} \dot{S}_{kk(2,\,0,\,0)} \right] + \frac{12}{d_\alpha^{(p)2}} Q_{1(1,\,0,\,0)} \tag{B4}$$

$$L_{2(0,\,0,\,0)} = \frac{h_\beta^2}{20}[-\rho c_p \dot{T}_4 + T_0 d_t \dot{C}_4] + \frac{1}{2} T_0 \alpha \left[\dot{S}_{kk(0,\,0,\,0)} - \frac{12}{h_\beta^2} \dot{S}_{kk(0,\,2,\,0)} \right] + \frac{12}{h_\beta^2} Q_{2(0,\,1,\,0)} \tag{B5}$$

$$L_{3(0,\,0,\,0)} = \frac{l_\gamma^2}{20}[-\rho c_p \dot{T}_5 + T_0 d_t \dot{C}_5] + \frac{1}{2} T_0 \alpha \left[\dot{S}_{kk(0,\,0,\,0)} - \frac{12}{l_\gamma^2} \dot{S}_{kk(0,\,0,\,2)} \right] + \frac{12}{l_\gamma^2} Q_{3(0,\,0,\,1)} \tag{B6}$$

It should be noted the interfacial quantity $L_{1(1,0,0)}$ has already been provided by Eq. (42).

The explicit expressions of the interfacial moisture flux quantities are given below

$$M_{1(0,\,0,\,0)} = -\frac{d_\alpha^{(p)2}}{20} \dot{C}_3 + \frac{12}{d_\alpha^{(p)2}} F_{1(1,\,0,\,0)} \tag{B7}$$

$$M_{2(0,\,0,\,0)} = -\frac{h_\beta^2}{20} \dot{C}_4 + \frac{12}{h_\beta^2} F_{2(0,\,1,\,0)} \tag{B8}$$

$$M_{3(0,\,0,\,0)} = -\frac{l_\gamma^2}{20} \dot{C}_5 + \frac{12}{l_\gamma^2} F_{3(0,\,0,\,1)} \tag{B9}$$

It should be noted the interfacial quantity $M_{1(1,0,0)}$ has already been provided by Eq. (50).

References

Aboudi, J., Pindera, M-J., Arnold, S.M., 1994. Elastic response of metal matrix composites with tailored microstructures to thermal gradients. Int. J. Solids Structures 31, 1393–1428.

Aboudi, J., Pindera, M-J., Arnold, S.M., 1995. A coupled higher order theory for functionally graded composites with partial homogenization. Composites Eng. 5, 771–792.

Goldberg, R.K., Hopkins, D.A., 1995. Thermal analysis of a functionally graded material subjected to a thermal gradient using the boundary element method. Composites Eng. 7, 793–806.

Johnson, J.N., Hixson, R.S., Gray, G.T., 1994. Shock wave compression and release of aluminum/ceramic composites. J. Appl. Phys. 76, 5706–5718.

Pindera, M-J., Dunn, P., 1997. Evaluation of a higher-order theory for functionally graded composites via the finite-element method. Composites, Part B: Engineering 28B, 109–119.

Sih, G.C., Michopoulos, J.G., Chou, S.C., 1986. Hygrothermoelasticity. Nijhoff, Dordrecht.

Springer, G.S. (Ed.), 1981. Environmental Effects on Composite Materials. Technomic, Lancaster.

Springer, G.S. (Ed.), 1984. Environmental Effects on Composite Materials, 2. Technomic, Lancaster.

Springer, G.S. (Ed.), 1988. Environmental Effects on Composite Materials, 3. Technomic, Lancaster.

Weitsman, Y., 1987. Stress assisted diffusion in elastic and viscoelastic materials. J. Mech. Phys. Solids 35, 73–93.

Weitsman, Y., 1995. Effects of fluids on polymeric composites—a review. Office of Naval Research, ONR Report under Contract No. N00014-90-J-1556.